3.1. Introduction to the Operational Oceanography

Operational Oceanography can be defined as the activity of systematic and long-term routine measurements of the seas and oceans and atmosphere, and their rapid interpretation and dissemination. Important products derived from operational oceanography are:

- nowcasts providing the most usefully accurate description of the present state of the sea including living resources
- forecasts providing continuous forecasts of the future condition of the sea for as far ahead as possible
- hindcasts assembling long term data sets which will provide data for description of past states, and time series showing trends and changes

Operational Oceanography proceeds usually, but not always, by the rapid transmission of observational data to data assimilation centres. There, powerful computers using numerical forecasting models process the data. The outputs from the models are used to generate data products, often through intermediary value-adding organisations. Examples of final products include warnings (of coastal floods, ice and storm damage, harmful algal blooms and contaminants, etc.), electronic charts, optimum routes for ships, prediction of seasonal or annual primary productivity, ocean currents, ocean climate variability etc. The final products and forecasts must be distributed rapidly to industrial users, government agencies, and regulatory authorities.

Marine Research and Development

Marine research and development that ranges from the fundamental through to the applied end of the spectrum will always be necessary to support operational oceanography. Ultimately, new systems based on new technology and new understanding of the sea will permit long range forecasts which will be of great benefit in managing the seas and oceans, and in predicting changes and variability of climate. The role of marine R&D does not cease once a fully operational regional oceanographic forecasting system is in place. The WMO and national meteorological organisations have demonstrated that strong investment in Research and Development to support the equivalent meteorological operational capabilities is required to maintain the viability of an operational programme.

Interaction between marine research operational oceanography box leads to mutual benefits on both sides. Not only will operational oceanography depend upon results and technology developed by marine research institutes but also marine science will profit greatly from

operationally acquired data and time series of the seas. Ultimately, these data might contribute to the development of new and complex ecosystem models that could one day allow a more precise forecast of living marine resources than is possible at present.
(according to the EuroGOOS definitions presented on the web site:
http://ioc.unesco.org/Oceanteacher/oceanteacher2/01_GlobOcToday/06_OpOc/OperationalOceanography.htm
More information could be found on the same site.)

3.1.1. Tools of operational oceanography.

3.1.1.1. Operational observations.

3.1.1.1.1. Remote Sensing of the Ocean from Space

1.PRINCIPLES AND METHODS OF SATELLITE OCEANOGRAPHY

1.1.INTRODUCTION

Why would anyone wish to study the sea from the space? There are few reasons, which are immediately apparent:

-to observe simultaneously large area covering few typical scales of oceanic phenomena;

-to observe one and the same place with the frequency of the corresponding to the process time scale;

-to study basin-wide phenomena*;*

- to obtain continuous long term data sets;

-to observe regions not easily studied by traditional methods;

-to observe regions not easily studied by traditional methods;

-to make measurements which are either impossible or difficult by ordinary means.

1.2. SIGNIFICANCE OF REMOTE SENSING DATA IN THE OCEAN OBSERVING SYSTEM

Oceans cover about two third of the Earth surface and a special ocean observing system should be developed for many practical needs. The ocean observing system should be able to provide continuous long-term data sets and basin-wide coverage. The frequency and spatial resolution of observations should be consistent to spatial and temporal scales of oceanic processes. This means that an area covering few typical scales of oceanic phenomena should be observed simultaneously and one and the same place need to be observed few times during the time scale of the most energetic oceanic processes. Traditional oceanographic methods do not satisfy that demands. Therefore new technologies are applied to fulfill basin-wide observations of the World Ocean.

Remote sensing of the ocean from space is considered now as one of the major sources of continuous data flow characterizing the state of the World Ocean and its variability as the satellite platform provides a means for global monitoring of various oceanic parameters. Instruments placed on the spacecraft usually have a broad viewing angle permitting to observe large areas of sea surface simultaneously. The rotation of the Earth results in the successive shift of the spacecraft path projection on the Earth surface and permits to cover the whole ocean by observations during a day. Long-term satellite datasets covering last 20 years are now available for use in the investigation of climate trends and variability.

The ocean remote sensing is based on measurements of natural or artificial radiation coming from the ocean surface. The electromagnetic radiation arriving at the spacecraft level depends from the state of the atmosphere and the ocean surface. However the knowledge of electromagnetic radiation formation and transfer is high to describe quantitatively its propagation through the atmosphere and its relation to the sea state. Therefore by the selection of the proper electromagnetic waves we can to obtain both qualitative and quantitative description of oceanic processes manifesting on the sea surface. The remote sensing of the ocean is based on the use of the radio frequencies and the natural light. Millimetric, centimetric and decimetric radio waves with the wavelength from one milimeter to 100cm are the most important for the space observations. The natural light in visible (0.4 – 0.7 μ m), near infrared (0.7-3 μ m) and thermal infrared (3 – 14 μ m) bands contains information about the sea state.

1.3.FORMATION AND TRANSPORT OF THE RADIATION

The formation and transport of the radiation in all bands is determined by the emission, absorption and scattering (Fig. 1.1). Let considered briefly all those processes.

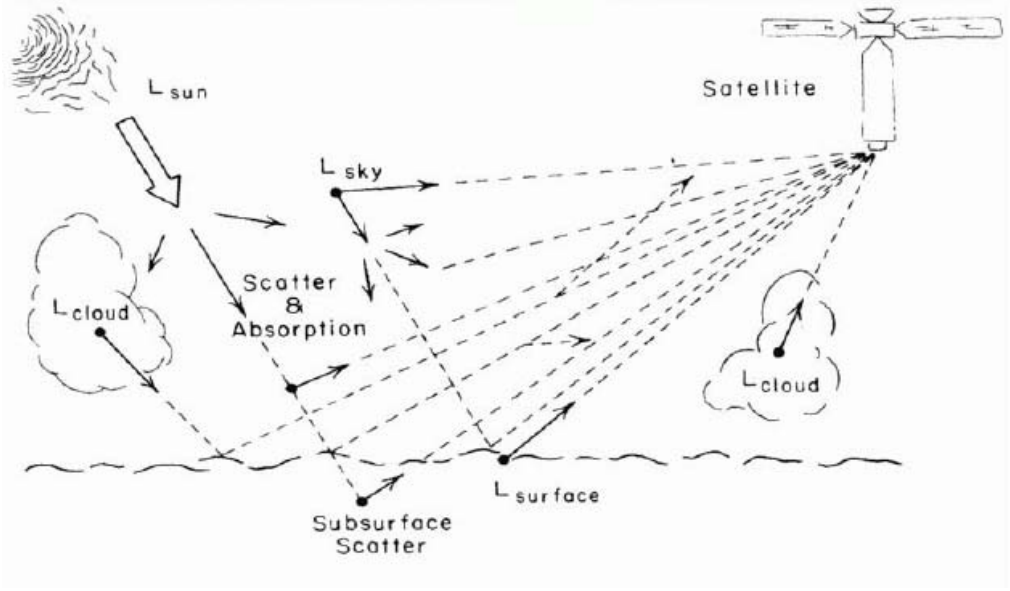

Fig. 1.1. The scheme of propagation of the natural light (After Stewart R. Methods of Satellite oceanography),

Absorption of the radiation

The primary mechanism for absorption by gases is the energy exchange between a matter and radiation. The radiation could raise the energy level of orbital electrons; induce vibration or rotational motion of the molecules. It is well known from the quantum mechanics that exchanges of energy between radiation and matter are quantized. Each possible level of orbital electrons, vibration or rotation of molecules has a distinct energy associated with it, and only radiation whose energy exactly matches the difference in energy between two states can be absorbed. As the energy quantum is proportional to the frequency of radiation the quantization results in an absorption spectrum, the absorption as a function of frequency that is composed of a set of narrow peaks or lines.

Emission of the radiation

The emission of the radiation for the idealised black body radiation is defined by the Plank's equation:

$$B(\lambda) = \frac{2 \cdot \pi \cdot c^2}{\lambda^5} \cdot \frac{1}{\exp\left[h \cdot c / \left(k \cdot T \cdot \lambda\right)\right] - 1},$$

where λ is the wavelength of the emitted radiation, T is the temperature of the black body, c is the light velocity, h and k are Plank and Boltzmann constants. However the most natural bodies emit radiation at a somewhat reduced rate with respect to that from a black body.

$$B^*(T) = \varepsilon \cdot B(T)$$

The ratio of the spectral radiance emitted by a real body relative to that emitted by a black body ε is named the spectral emissivity. An example of the natural source of radiation gives the sun. The spectral radiation from the sun is approximated by the best-fitting curve of radiation from a black body at 5900 K (Fig.1.2).

The rate at which a matter absorbs radiation and the rate at which radiation is emitted are not independent. The Kirchoff's law states that matter in the local thermodynamic equilibrium must emit at the same rate that it absorbs. This means that the spectral emissivity is equal to the spectral apsorptance

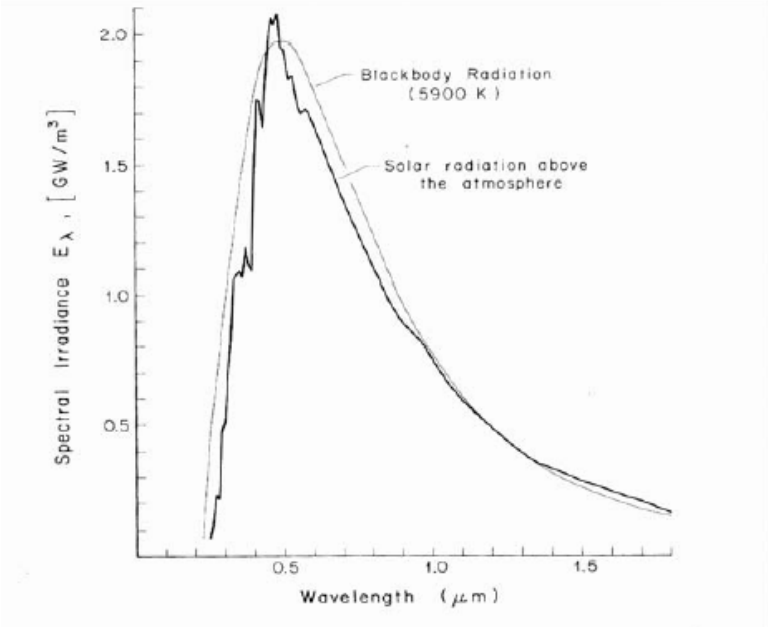

Fig. 1.2. Spectral irradiance from the sun and the blackbody radiance at 5900K. (After Stewart R. Methods of Satellite oceanography)

Scattering of the radiation

Radiation passing through the atmosphere scattered by different molecules and particles including the water drop of fog, clouds, rain and the solid particles of smoke and haze. If particles are sparse, scatter primarily changes the angle of propagation. If particles are sufficiently dense, the radiation is scattered again and again (Fig. 1.3) partly obscuring the image of the radiating object. Scattering is significant if the radiation wavelength has the same order of magnitude or less than a particle size.

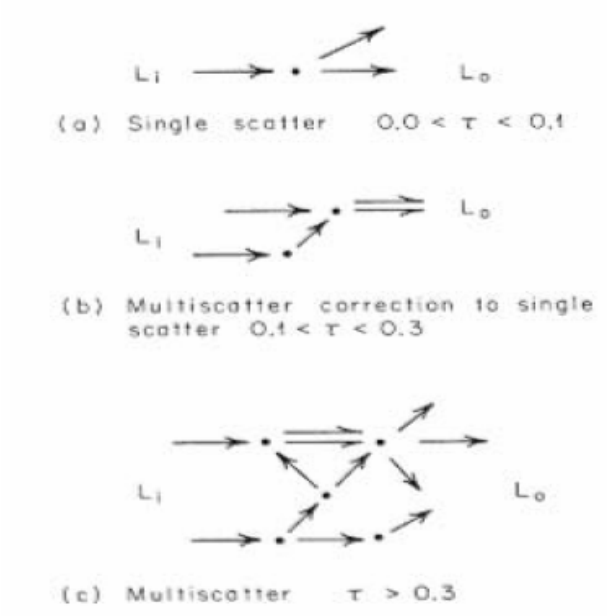

Fig. 1.3. Scattering by particles of different density. (After Stewart R. Methods of Satellite oceanography)

The distribution of the scattered radiance with angles is described either by phase function or by the volume scattering function (Fig. 1.4). The phase function is the volume scattering function normalized to the total volume scattering. Both forms of the description of the scattered radiation are used as for the scattering by the single particle and for the scattering by the ensemble of particles.

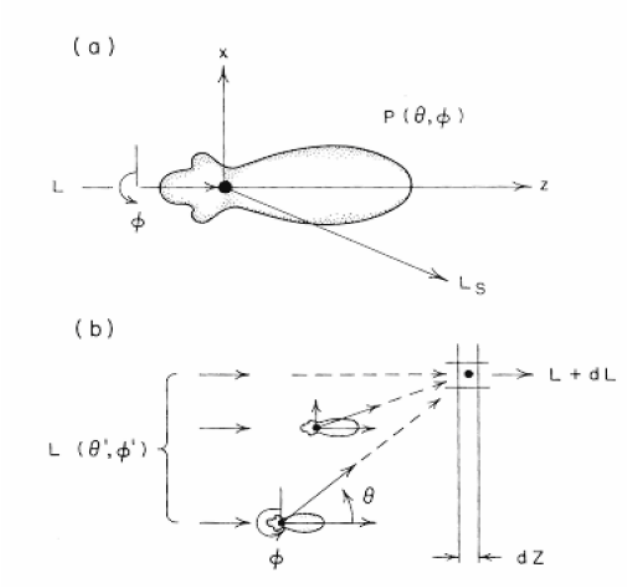

Fig. 1.4. The volume scattering function defines redistribution of light (a) and how the scattered light goes to the to the selected volume. (After Stewart R. Methods of Satellite oceanography).

Radiation transfer equation

Given the scattering and absorbing property of particles it is possible, in principle, to calculate the influence of particles on radiation propagating through atmosphere using radiation transfer equation. In practice, the calculations are exceedingly difficult, and many techniques have been proposed for finding approximate solution of the radiation transfer. We consider simple double-flux approximation of the radiation transfer equation.

Radiation transfer equation in two-ray approximation; optical thickness

Let assume that the radiation propagates along axes Z and the scattering occurs only in back and forward directions. Let consider two-wavelength dependent beam of radiation $F_+(z)$ and $F_-(z)$ propagating in positive and negative directions. The flow $F_+(z)$ is attenuated within the infinitesimally small element dz due to absorption and scattering of the radiance in the back direction:

$$dF_+ = -(k+s)\cdot F_+ \cdot dz$$

where k and S are absorption and scattering coefficients. However $F_+(z)$ not only attenuated but also increased due to the back scattering of $F_-(z)$ and thermal emission. Therefore finally we have

$$\frac{dF_+}{dz} = -(k+s)\cdot F_+ + s\cdot F_- + k\cdot F_r$$

where F_r is a black body radiation with the temperature of the matter in the volume. The same type of equation could be written for the radiation propagating in the negative direction

$$\frac{dF_-}{dz} = (k+s)\cdot F_- - s\cdot F_+ - k\cdot F_r$$

Absorption and scattering coefficients depend in general from z. Therefore it is comfortable to introduce new variable, optical thickness, for the layer between z_1 and z_2 by the following way

$$\tau(z_1, z_2) = \int_{z_1}^{z_2} (k+s)\cdot dz$$

Then the radiation transfer equation rewrites by the following form

$$\frac{dF_+}{d\tau} = -F_+ + \omega\cdot F_- + (1-\omega)\cdot F_r$$

$$\frac{dF_-}{d\tau} = F_- - \omega\cdot F_+ - (1-\omega)\cdot F_r$$

Let us consider in details the case when radiation propagates through the layer with optical thickness τ_0, coefficients in the latter system are constant and the emission could be neglected. Let the downwelling radiation on the surface of the layer is equal to F_0, and on the bottom of the layer when $\tau = \tau_0$ the upwelling radiation is equal zero. Then

$$F_+(0) = F_0, \quad F_-(\tau_0) = 0$$

General solution of the radiation transfer equation has the form:

$$F_+ = A_+\cdot e^{\lambda_+\cdot\tau} + A_-\cdot e^{\lambda_-\cdot\tau}$$

$$F_- = B_+\cdot e^{\lambda_+\cdot\tau} + B_-\cdot e^{\lambda_-\cdot\tau}$$

and coefficients $A_\pm$ and $B_\pm$ satisfy the following system of equations:

$$(\lambda+1)\cdot A - \omega\cdot B = 0$$

$$\omega \cdot A + (\lambda - 1) \cdot B = 0$$

Therefore

$$\lambda_{\pm} = \mp\sqrt{(1-\omega^2)} = \mp\gamma$$

and

$$B_{\pm} = \frac{\omega}{(1 - \lambda_{\pm})} \cdot A_{\pm}$$

The boundary conditions are used to define $A_{\pm}$. We have

$$A_{+} + A_{-} = F_0$$

$$\frac{\omega}{1+\gamma} \cdot A_{+} \cdot e^{-\gamma \cdot \tau_0} + \frac{\omega}{1-\gamma} \cdot A_{-} \cdot e^{\gamma \cdot \tau_0} = 0$$

Finally

$$F_{+} = F_0 \cdot \frac{sh[\gamma \cdot (\tau_0 - \tau)] + \gamma \cdot ch[\gamma \cdot (\tau_0 - \tau)]}{sh(\gamma \cdot \tau_0) + \gamma \cdot ch(\gamma \cdot \tau_0)}$$

$$F_{-} = F_0 \cdot \frac{\omega}{sh(\gamma \cdot \tau_0) + \gamma \cdot ch(\gamma \cdot \tau_0)} \cdot sh[\gamma \cdot (\tau_0 - \tau)]$$

Using those formulae we found

$$\frac{F_{+}(\tau_0)}{F_0} = \frac{\gamma}{sh(\gamma \cdot \tau_0) + \gamma \cdot ch(\gamma \cdot \tau_0)} = \frac{2 \cdot \gamma \cdot e^{-\gamma \cdot \tau_0}}{(1+\gamma) - (1-\gamma) \cdot e^{-2 \cdot \gamma \cdot \tau_0}}$$

i.e. downwelling radiation partially passes through the layer. Therefore the latter expression is named as the transmission coefficient. By the same way we found the upwelling radiation on the top of the layer and the fraction

$$\frac{F_{-}(0)}{F_0} = \frac{\omega \cdot sh(\gamma \cdot \tau_0)}{sh(\gamma \cdot \tau_0) + \gamma \cdot ch(\gamma \cdot \tau_0)} = \frac{\omega \cdot (1 - e^{-2 \cdot \gamma \cdot \tau_0})}{(1+\gamma) - (1-\gamma) \cdot e^{-2 \cdot \gamma \cdot \tau_0}}$$

is named as the reflection coefficient. Both coefficients are functions of the wavelength.

Sun radiation spectrum on the Earth surface; transparency windows in the atmosphere.

An example of the layer, which attenuates and reflects the radiation, is the atmosphere. Particularly, the sunlight is transformed significantly passing through the atmosphere (Fig. 1.5).

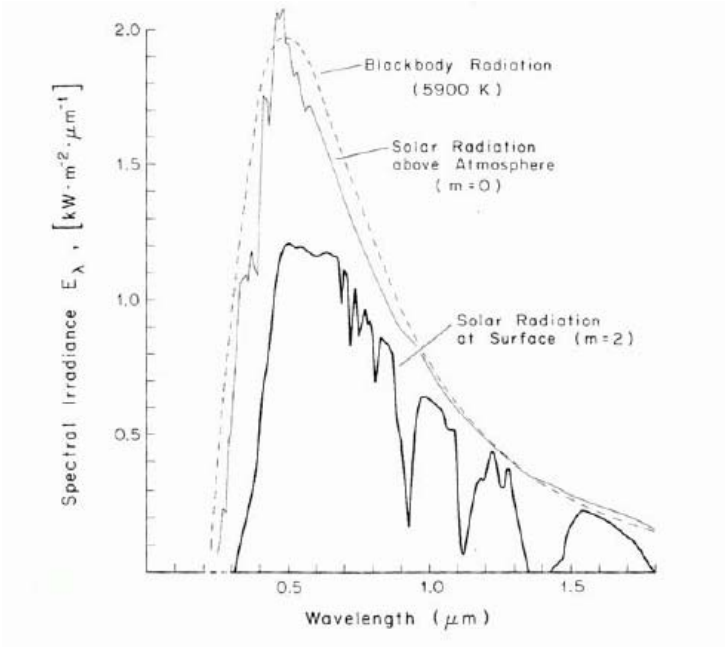

Fig. 1.5. Solar radiation at the surface of the Earth (After Stewart R. Methods of Satellite oceanography).

We can find however that for some wavelength the attenuation of the sunlight is not so strong (Fig. 1.6). Therefore we have some transparency windows in the atmosphere where the attenuation of the radiation is moderate.

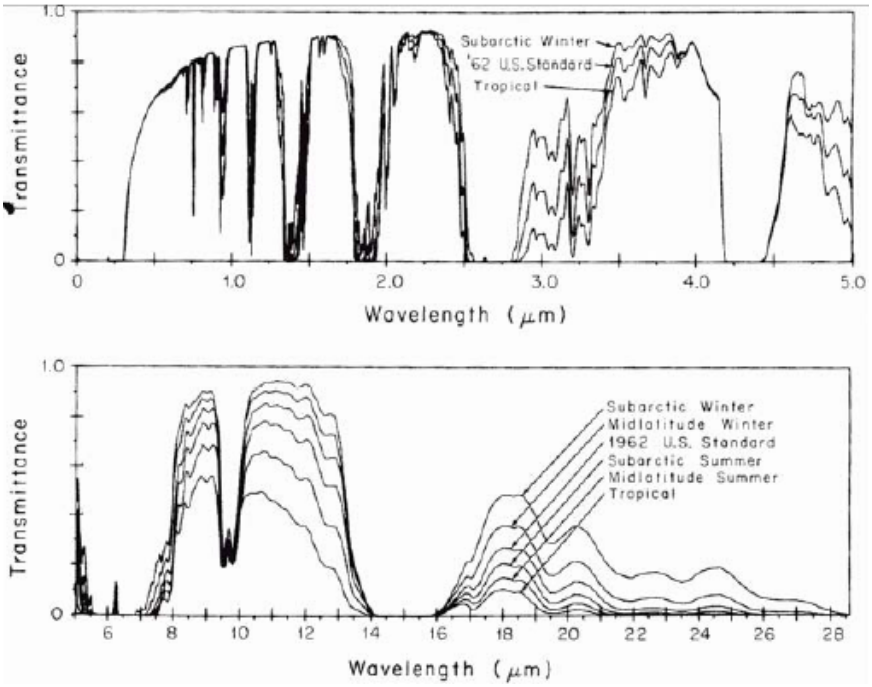

Fig. 1.6. Atmospheric transmission for different wavelengths (After Stewart R. Methods of Satellite oceanography).

The transparency windows permit to use efficiently the remote sensing methods for the oceanographic investigations.

1.4.INTERACTION OF THE RADIATION WITH THE SEA

Emission of the radiation from the sea surface

The radiation emitted by the sea surface depends from the sea surface temperature (SST) according to the Plank formula. However the emission coefficient of sea surface itself depends from the temperature and salinity of seawater, sea surface roughness and the angle of observation. This dependence is weak in visible and IR bands where the emissivity coefficient is close to unity. However for radio waves the emissivity coefficient is rather sensible to variations of the sea surface state. This dependence is used for remote measurements from space.

Scattering of the light in the water.

The major part of sunlight is reflected from the surface. The reflection follows to the rule that incident angle is equal to the reflecting angle. Even waving surface follows this rule only modulating the reflecting angle according to the slope of the sea surface. Observations of the sun glint are used for the determination of the surface wave spectrum using aircraft measurements. The sun glint area is just excluded from observations from spacecraft.

The reminding sunlight is transmitted through the ocean interface and propagates to the depth. The light propagation below the sea surface is described by the same radiation transfer equation, which is considered above. Chlorophyll cells and dissolved matter absorb some part of the light. Another one is scattered on molecules and suspended particles forming upward propagating radiation. Mainly the sunlight is attenuated in upper tenth meter but it reflects from the bottom in the shallow water. Backscattered light partly transmits through the sea surface and contains information about dissolved and suspended matter. This scattered light constitutes few percents of the incident sunlight.

Scattering of radio waves by the rough sea surface

Radio waves transmitted to the sea surface are scattered in many directions after striking the sea. A small portion of this scattered energy, carrying with it information about phenomena at the surface, is eventually scattered backward. For angles of incidence near vertical, scatter comes from mirror-like facets that reflect energy approximately as from a plane surface even if the real sea surface is covered by waves. Away from the vertical, the number of facets rapidly becomes very small, because almost no wave have slope greater than 25°. At greater angles, another mechanism reflects energy toward the receiver, resonant scatter from single sinusoidal component of the spectrum of oceanic waves that match the projected wavelength of the radio signal onto the sea surface. Surfaces with a regular lattice of roughness act exactly like a

diffraction grating. Because scatter from the repeating lattice pattern add coherently far from the surface, the scatter is resonant. The resonant scatter is often named Bragg scatter. The Bragg equation

$$\vec{k} = 2 \cdot \vec{k}_r \cdot \sin \theta$$

connects wave vector of the surface wave $\vec{k}$ with the electromagnetic wave vector and incident angle. The intensity of the backscattered signal is proportional to the surface wave energy. Therefore the modulation of the surface gravity waves produce the means for observations of different processes on the sea surface.

1.5.MAJOR METODS OF THE OCEAN REMOTE SENSING

Observation of the ocean from space is carrying out using the wavelength where the radiation dependens from the characteristics of the sea surface and the atmosphere is transparent or the atmospheric influence could be corrected accurately. There are two groups of methods, which are used now for remote sensing of the ocean. The first one is based on the observation of natural radiation. The most popular is the use of the visible light from the sun. Visible band observations could have very high spatial resolution, up to tens of centimeter, but they should be fulfilled at the daytime and at the cloud-free conditions. Since the scattering of visible light in the atmosphere is significant, haze, fog and atmospheric aerosols contaminate visible band observations. Therefore the most efficient are observations in the clear atmosphere and the major problem of quantitative description of the sea surface is the correction of atmospheric scattering. Multi-channel measurements are used to reduce the atmospheric influence and to characterize quantitatively the ocean surface.

The thermal radiation of the sea surface at the IR band is used for observation of thermal contrasts on the ocean surface. IR radiometers typically could have resolution from few hundred meters to one kilometer. IR observations also limited by clouds and in general absorption and emission in the atmosphere contaminates significantly the signal coming from the ocean. However the special choice of wavelength in transparency windows permits to reduce the atmospheric impact. Therefore IR remote sensing is very efficient way to observe oceanic processes. Multi-channel IR remote sensing is used to correct atmospheric effects and to measure the sea surface temperature.

Radio frequencies are free from the major drawback of visible band and IR remote sensing, as clouds are practically transparent for radio waves. However the receiving antenna should be very large to achieve high spatial resolution and its size grows with the wavelength. Therefore remote sensing of the ocean is restricted by milimetric to decimetric wavelengths.

Typical special resolution of the radiometers using radio frequencies is from few to hundred kilometers. The receiving radiation could depend from the state of atmosphere as clouds with high water content and rain still distort the signal coming from the oceanic surface. Therefore an accurate interpretation of the microwave imagery should be based on the concomitant information, which could be for example the data from another channel. Measurements of the sea surface temperature, sea surface salinity and sea surface wind are based on the use of multi-channel data.

The second group of methods is based on the active location of the sea surface using radio frequencies. Clouds are transparent for the active location and the ocean could be observed practically for all weather conditions.

Radiation of the radar pulses to the Earth surface exactly downward and receiving of the mirror reflected signal is the principles of operation of the space altimeter. Measuring the time required for the pulse transmission from the altimeter antenna to the Earth surface and back permits to calculate the height of the satellite. Since the velocity of the light depends from the atmosphere state, altimeter complex includes microwave radiometer permitting to evaluate the water vapor content in the atmosphere. Transmission of pulses at nadir restricts the altimeter measurements to the along track.

The radar pulses transmission at sliding angles and reception of the back scattering signal from the ocean surface is the principle of operation the real aperture radar and the radar with synthetic aperture. Both instruments provide scanning image with spatial resolution up to one km for the real aperture radar. The synthetic aperture radar uses the coherent signal and measures phases of the scattered signal. The movement of the satellite and processing of sequential observations one and the same area permits to increase spatial resolution, which is up to ten meter.

The special radar designed to measure the surface wind is named as the scatterometer. The scatterometer measures the back scattering signal at two beams, which permits to determine both the wind speed and the wind direction. The following bands of electromagnetic waves which are used in the ocean remote sensing are presented at the Tables below.

A relevant choice of satellite orbit is significant part of the ocean remote sensing mission. Three special types of orbit are used for the ocean remote sensing. Sun-synchronic orbits pass the Earth at the same local time. The choice of this orbit is efficient when the visible or IR band observations are carrying out. Exact repeating orbits pass comes exactly through the same line over some period of time. This type of orbit is used for the along track measurements and the time of the repeating of orbits is found from the compromise between the spatial and temporal resolution. The use of geostationary orbits is rather limited in the ocean remote sensing as the

geostationary satellites observe the Earth from the large height about 36000 km. The geostationary satellites hang over the same point above the Earth and its major advantage consists in the possibility to observe large area of the ocean with high temporal resolution. However it is hard to achieve the relevant spatial resolution of instruments on the surface from the large distance above the Earth. The remote sensing of the ocean have developed intensively during the last two decades. The last decade is characterizing by the transition from the experimental to operational remote sensing of the ocean.

Nomenclature of Light Bands

Frequency Range (Hz)	Adjectival Designation	Wavelengths (mkm)
0.3×10^{12} – 3.0×10^{12}	Far Infrared	100 – 1000
3.0×10^{12} – 2.0×10^{13}	Middle Infrared	14 – 100
2.0×10^{13} – 1.0×10^{14}	Thermal Infrared	3 – 14
1.0×10^{14} – 4.3×10^{14}	Near Infrared	0.7 – 3
4.3×10^{14} – 7.5×10^{14}	Visible Light	0.4 – 0.7
7.5×10^{14} – 3.0×10^{16}	Ultraviolet Light	0.01 – 0.4

Nomenclature of the Radio Frequency Bands

Frequency Range	Metric subdivision	Adjectival Destination	Wave Length
3 – 30MHz	Decametric Waves	High Frequency	10 – 100m
30 – 300MHz	Metric Waves	Very High Frequency	1 – 10m
300 – 3000MHz	Decimetric waves	Ultra High Frequency	10 – 100cm
3 – 30GHz	Centimetric waves	Super high Frequency	1 – 10cm
30 – 300GHz	Millimetric waves	Extremely high frequency	1 – 10mm

2. OBSERVATION OF OCEANIC PROCESSES BY SCANNER IMAGERY

The first and the most evident application of the remote sensing methods is their use for observations of oceanic processes. Scanning imagery from space provides unique possibility to observe large areas of sea surface and even to trace their temporal evolution. Observations of oceanic processes from space do not demand complex preprocessing but assume good physical understanding of the signal formation and its contamination.

2.1. NATURAL EMISSION OF RADIATION BY THE OCEAN

The seawater emits the radiation almost as a blackbody at visible and infrared wavelength (emissivity is about 0.98 – 0.99). Therefore IR observations in the atmosphere transparency windows are used for observations of thermal contrasts at the sea surface.

Non-homogenous distribution of the sea surface temperature (SST) permit to identify on IR scanner imagery position of jets and eddies. Fig. 2.1 presents image of the Black Sea obtained from AVHRR at the thermal IR band. The cyclonic Rim Current belting the sea along the coast is seen on Fig. 2.1 as the boundary between the light and dark tones. The light tone corresponds to the relatively warm water and the dark one to the cooler water near the coast. Large mesoscale eddies are also evident on this figure to the East and to the West from Crimea peninsula. Intense meandering of the Rim Current jet and some smaller scale eddies is seen to the North from Anatolian coast.

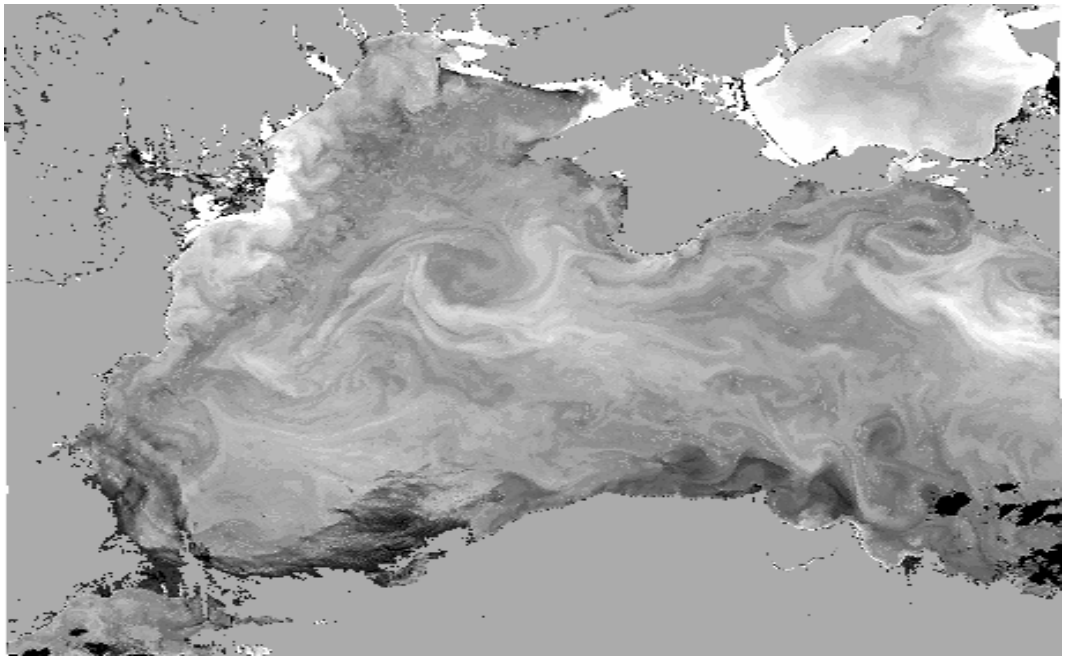

Fig. 2.1. Eddies and jets at the Black Sea observed by the AVHRR scanner

Another example is presented on Fig. 2.2 resulting from the map obtained by IR radiometer operating on the MODIS satellite. The Gulf Stream is shown on this figure as a warm jet propagating along the coast of United States until the Cap Hatteras. The Gulf Stream leaves

the coast near the Cap Hatteras and is seen as a front between the warm and the cold water. Another front corresponding to the Labrador current well shown to the North from the Gulf Stream.

Fig. 2.2. SST map of the Gulf Stream obtained by the MODIS.

Current jets are manifested on the IR scanner imagery because they are connected with thermal fronts due to the geostrophic relation (Fig. 2.3.).

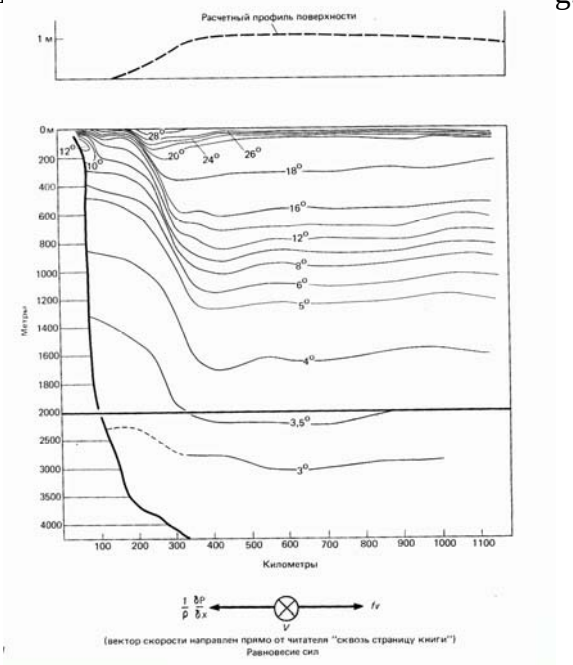

Fig. 2.3. Cross-section of the Gulf Stream. The velocity direction and geostrophic balance are shown at the bottom of figure.

Strong meanders of the Gulf Stream evident on Fig. 2.2 sometimes detached from the jet and form intense mesoscale eddies, so called cold and warm Gulf Stream rings. The set of IR images permit to consider the evolution of the Gulf Stream rings in details (Fig. 2.4). Eddies

similar to the Gulf Stream Rings are seen on the images because they transport at their center the water from other side of the front, which has another temperature. For example the water in the center of the ring shown on Fig. 2.4 has higher temperature with respect to the ambient water.

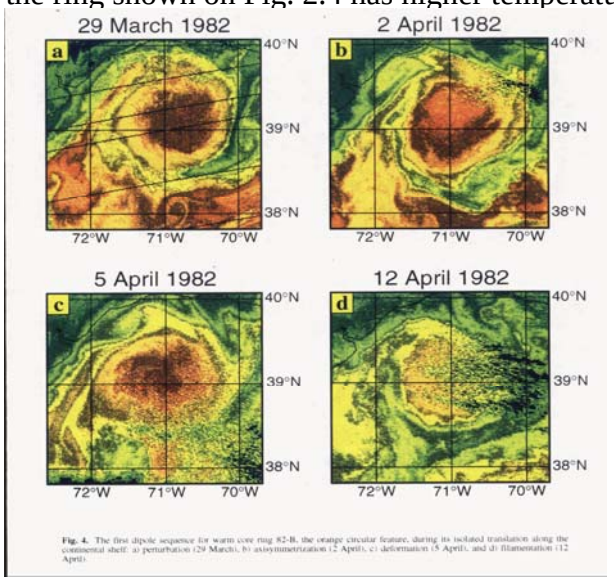

Fig. 2.4. Evolution of a warm core Gulf Stream Ring according to AVHRR data

Thermal contrasts in the IR imagery could be observed also in the open ocean, far from intense currents. Those contrasts appear due to some fine features of the upper ocean thermal structure and reflects some peculiarities of the air-sea interaction.

Usually the upper ocean thermal structure is presented by the quasi-homogeneous layer produced by the turbulent mixing induced by the instability of drift currents, breaking of surface and internal gravity waves or convection. The seasonal thermocline with low level of turbulence is situated on the bottom of the quasi-homogeneous layer on the depth from tenth to hundred meters.

However this simplified scheme should be applied carefully for the interpreting of IR remote sensing observations. The problem is that IR radiation is emitted by the thin layer just below the ocean surface. The depth of this layer has the same order of magnitude as the radiation wavelength. Therefore IR imagery under some conditions could reflect small-scale processes developing below the ocean surface.

One of the small-scale phenomenons influencing the IR observations is the skin layer. The skin layer is settled down in few millimeters below the sea surface. The temperature within the skin layer decreases to the surface since evaporation and long wave radiation are concentrated in few upper millimeters. There are three regimes of the ocean skin layer. The first regime is observed when the surface wind is very weak and surface waves are stable. The skin layer is well pronounced in this case and the temperature jump through the layer could achieve 1K. The second regime is developed under moderate winds when the surface waves are still

stable but the turbulence reduces the thickness of the layer and the temperature jump across of it. The third case corresponds to strong winds when the breaking of the short gravity waves destroys the skin layer and the surface temperature is the same as in the upper few meters. Let consider now the area of the open ocean where the quasi-homogeneous layer could be uniform in space on the scale of about thousand km. Then the non-homogenous weather conditions over that area could produce spatial contrasts on the IR image.

Another effect which should be considered when one interprets IR observations is connected with the diurnal cycle of the temperature in the upper layer of the ocean. A diurnal thermocline, which is formed at the daytime in the upper meter of the sea, could induce a few degrees difference of SST and modulate IR radiation under the calm weather conditions. Diurnal cycle of SST is well seen from continuous observations of the IR radiometer displaced on geostationary satellite (Fig. 2.5). This example shows also the advantage of geostationary satellites for oceanic remote sensing as the polar orbit satellite could not produce accurate observation of the diurnal cycle of SST.

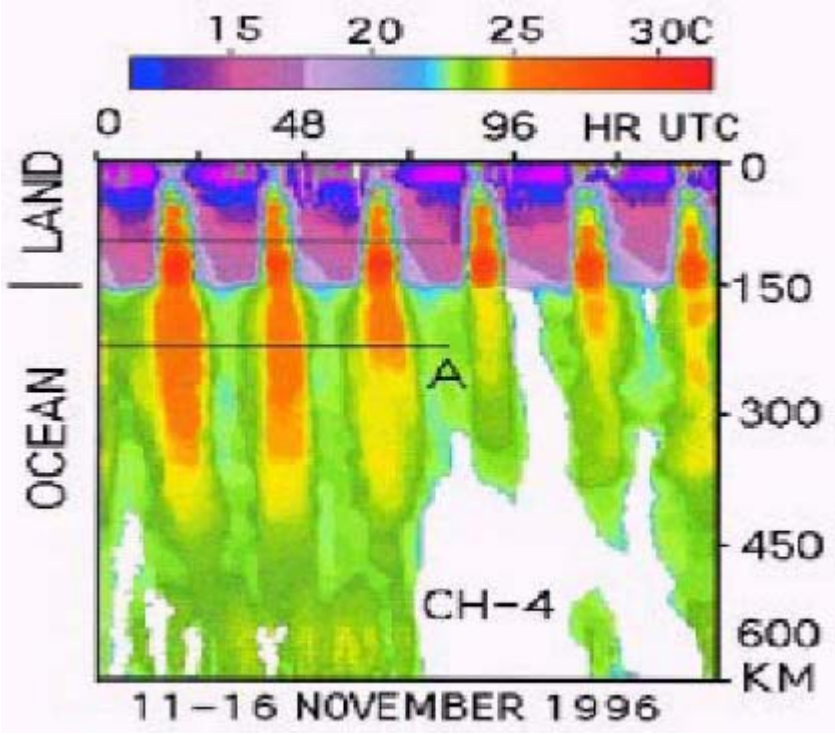

Fig. 2.5. Duirnal cycle of SST observed by Goes-8 satellite

However diurnal thermocline is formed only when the surface wind is weak enough and wind-induced turbulence incapable to mixed the whole quasi-homogeneous layer. Stronger wind destroys the diurnal thermocline and distributes the heat through the whole depth of the quasi-homogeneous layer. Thus again a contrast on the IR image could be induced by the spatially non-homogeneous surface wind.

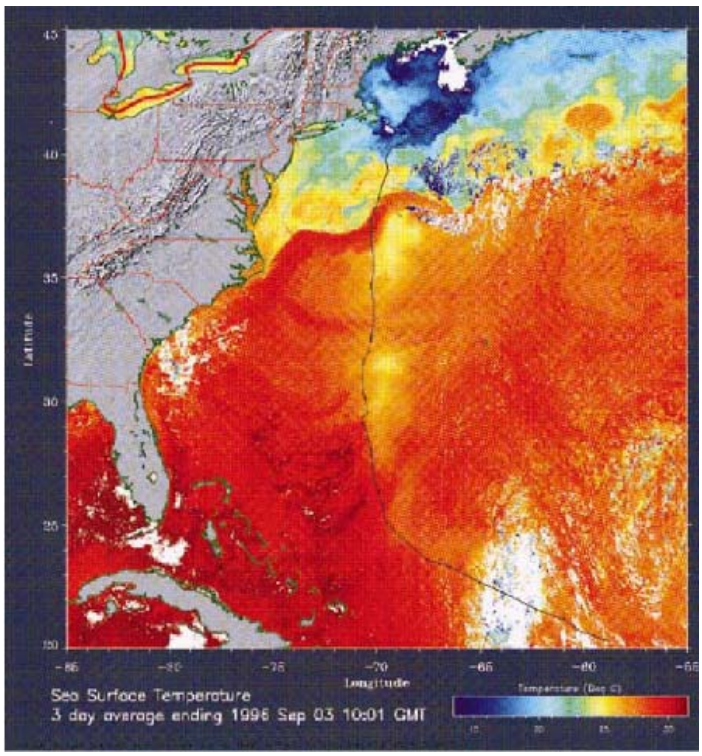

Fig. 2.6. Composite map of SST for few days after passing through the area of the hurricane Edwards

A very intense surface wind producing by the strong hurricane could deepen the seasonal thermocline due to the significant increase of the turbulent mixing within the quasi-homogeneous layer. Therefore the spatial non-homogeneous distribution of SST should be observed across the path of hurricane. The image on Fig. 2.6 presents the composite map of SST for few days after passing through the area of the hurricane Edwards obtained by IR radiometer from geostationary satellite. The pool of cold water is evident along the track of the hurricane.

The cooler water appearance along the track of hurricane is explained by the following way. A hurricane wind increases the level of turbulent energy in the mixed layer and the cold water from below of seasonal thermocline is entrained to the mixed layer. The entrainment of the cold water results in decrease of SST.

A wind blowing along the coast could be the reason of the non-uniform SST distribution well observed on IR images. One example of the cold-water appearance on the surface near the Crimea coast is well seen on Fig. 2.7 as a dark patch. The rise of the cold water to the surface has the following reason. Along coast wind induces offshore Ekman drift and warm surface water is replaced by cold water from below of the mixed layer not due the entrainment but just due to the intense vertical motion (Fig. 2.8).

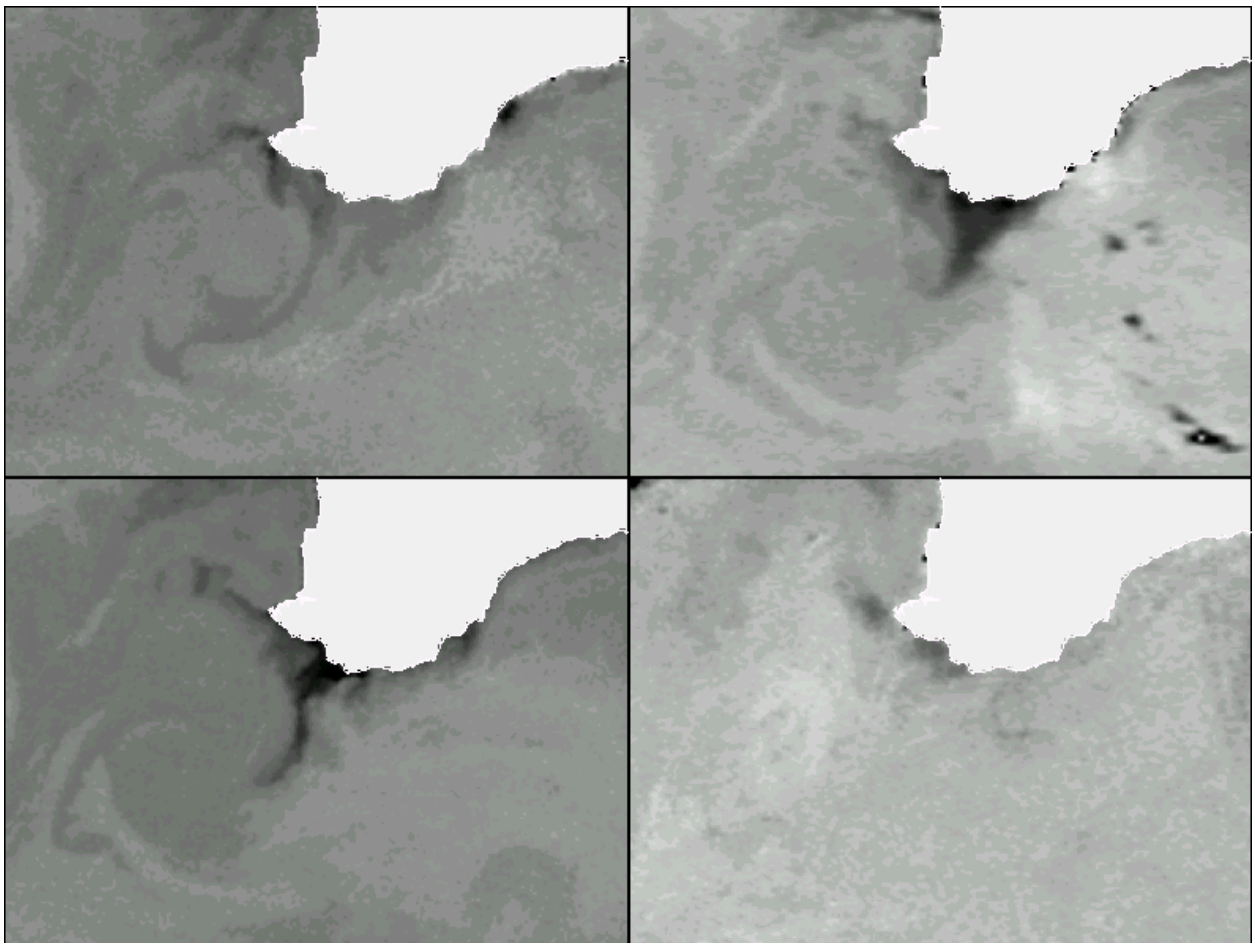

Fig. 2. 7. Manifestation of the coastal upwelling near the Crimea peninsula.

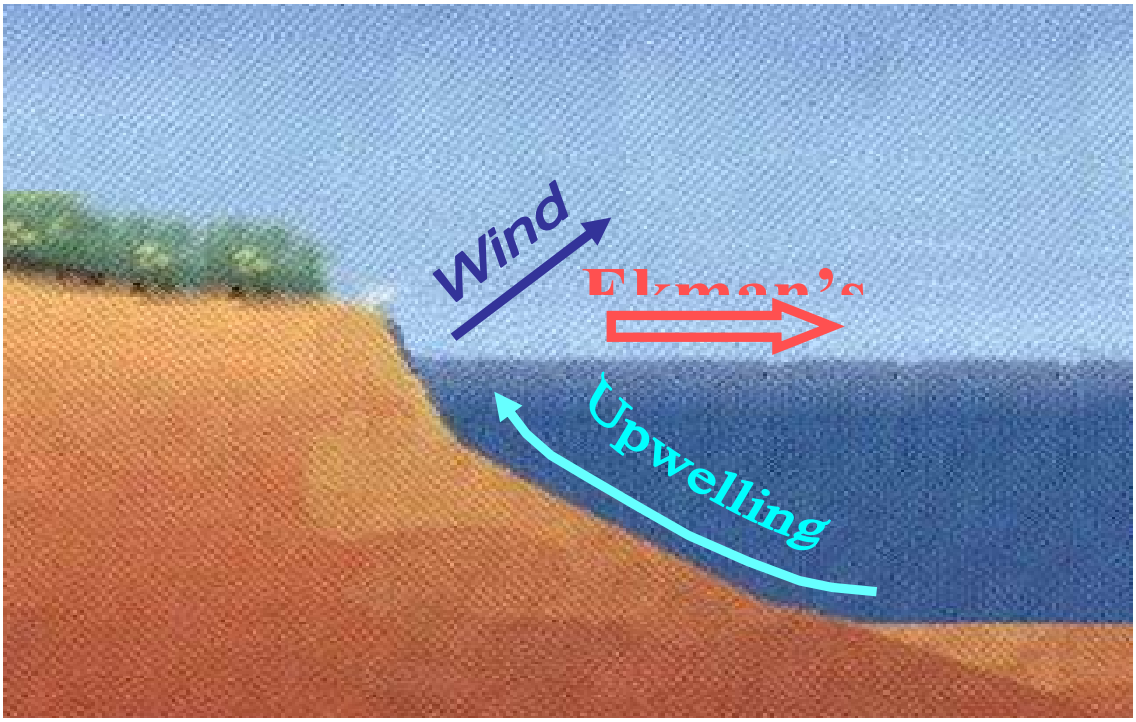

Fig. 2.8. How the along shore wind induces the coastal upwelling.

2.2UPWELLING RADIANCE IN VISIBLE BAND.

Visible band observations use the sun as the source of radiation. Therefore observations are available only at the daytime. Therefore if some part of the sea surface is covered by ice, a significant contrast is formed on visible band image of the sea surface since snow and ice only weakly absorb radiation. The sequence of visible band images permit to observe changes of ice sheets as it is shown on Fig. 2.9, obtained by the visible band scanner MOS in April 1998 in the area of Riga bay. Ice sheets are seen as white patches surrounded by the water which is black on the visible band image.

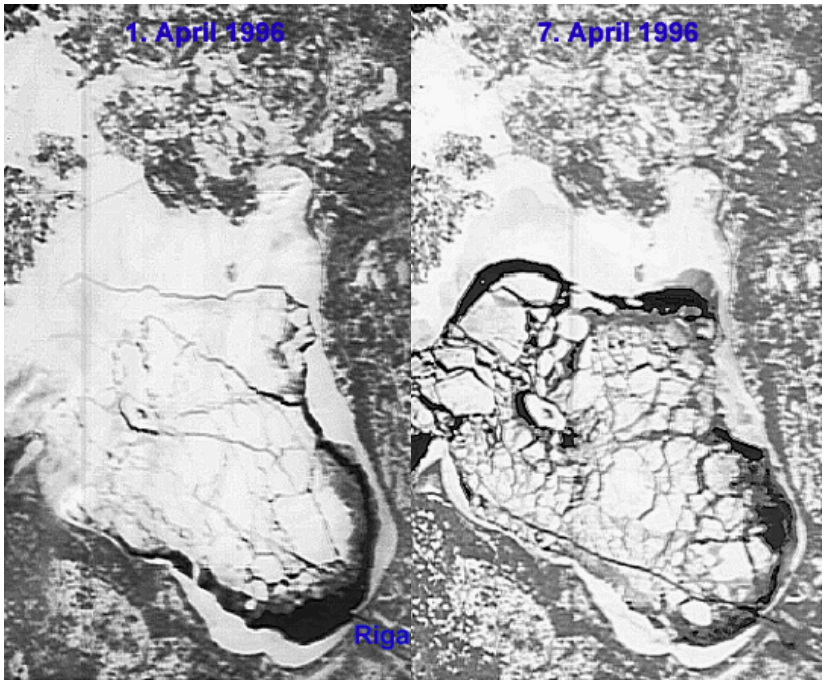

Fig. 2.9. Ice sheet evolution in the area of the Riga bay.

The signal in the open ocean depends on the amount of absorbing and scattering materials. Therefore it should be spatially non-homogenous and different dynamical structures are presented on the visible band imagery. The image presents on Fig. 2.10 shows the set of structures, which are manifested in the AVHRR visible channel image obtained on the wavelength 0.55 μ m. The scattering prevails in formation of signal on this wavelength.

Another example, shown on Fig. 2.11, presents the jet structure, which is manifested on the image due to the difference in absorption of the sunlight. The difference in absorption is produced by the phytoplankton blooming and following its transport by current. The image on Fig. 2.11 is obtained by MODIS scanner near the Patagonia and shows current situated offshore the South America..

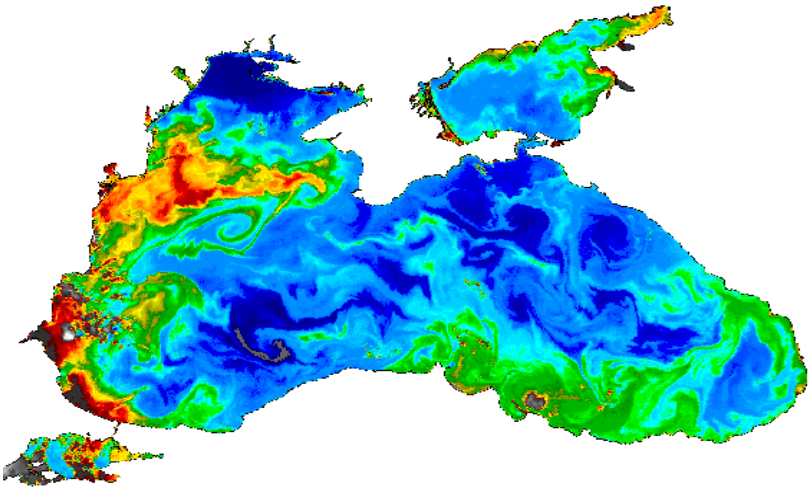

Fig. 2.10. Coccolithophores bloom in the Black Sea. Coccolithophores and their scales (coccoliths) cause reflection.

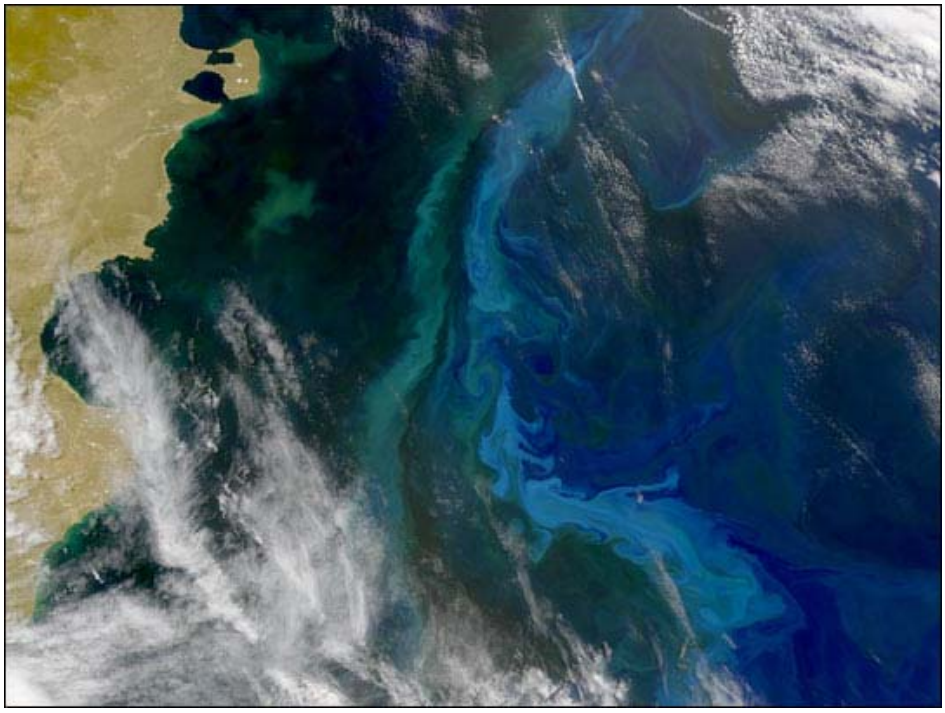

Fig. 2.11. The jet structure near the Patagonia, which is manifested on the visible band image due to the difference in absorption of sunlight.

The intense synoptic coastal upwelling could induce a booming of the plankton. The reason of the blooming in this case is the rise to the surface deep water, which is rich by biogenic elements. The upwelling onset could be found from the IR image of the same place as the patch of the cold water rising to the ocean surface. Fig. 2.12 shows the example of simultaneous observations near the Pacific coast of Canada and USA in visible band by the color scanner SeaWiFS and the sea surface temperature distribution on AVHRR image. There is an evident correlation of a high phytoplankton concentration and cold-water patches on the sea surface.

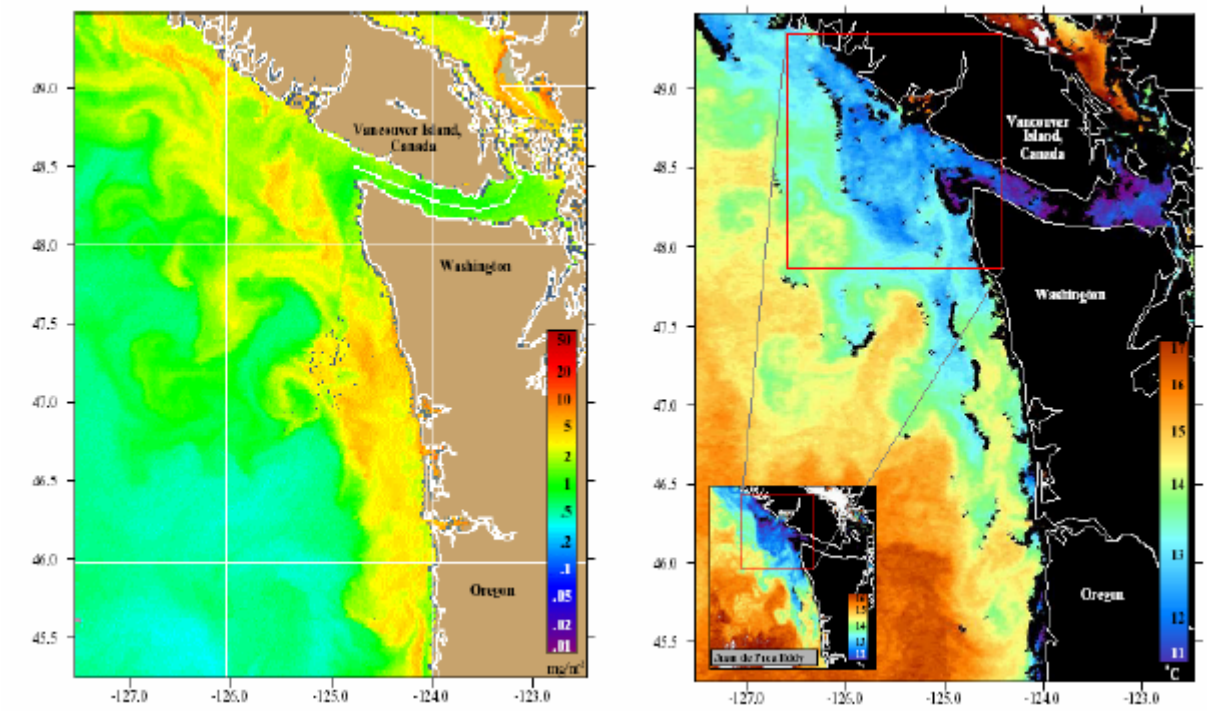

Fig. 2.12. Simultaneous observations near the Pacific coast of Canada and USA in visible band by the color scanner SeaWiFS and the sea surface temperature distribution on AVHRR image.

The similar example is presented on Fig. 2.14 in the Black Sea. The coastal synoptic upwelling is observed on the AVHRR image near the Turkish coast as the black strip. The simultaneous SeaWiFS image shows increased chlorophyll concentration exactly at the same place. The reason of the local blooming of phytoplankton is again the supply to the sea surface of the rich deep water.

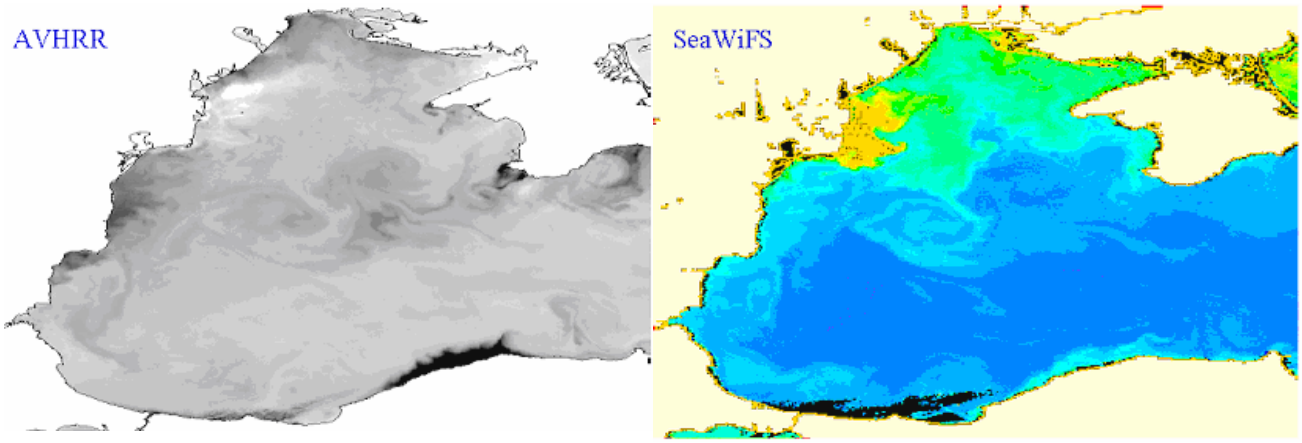

2.12. Coastal upwelling near Anatolia observed by IR and visible band scanners

2.3. ACTIVE LOCATION OF THE OCEAN SURFACE UNDER SLIDING ANGLES

Surface waves and wind: polar mesoscale cyclone in SAR imagery

Modulation of the radar signal by wind intensity and larger scale surface gravity waves provides informative footprint of the polar mesoscale cyclone (PMC) in SAR signal. Typical structure of the cyclone is presented in cloud visible band image (Fig. 2.13).

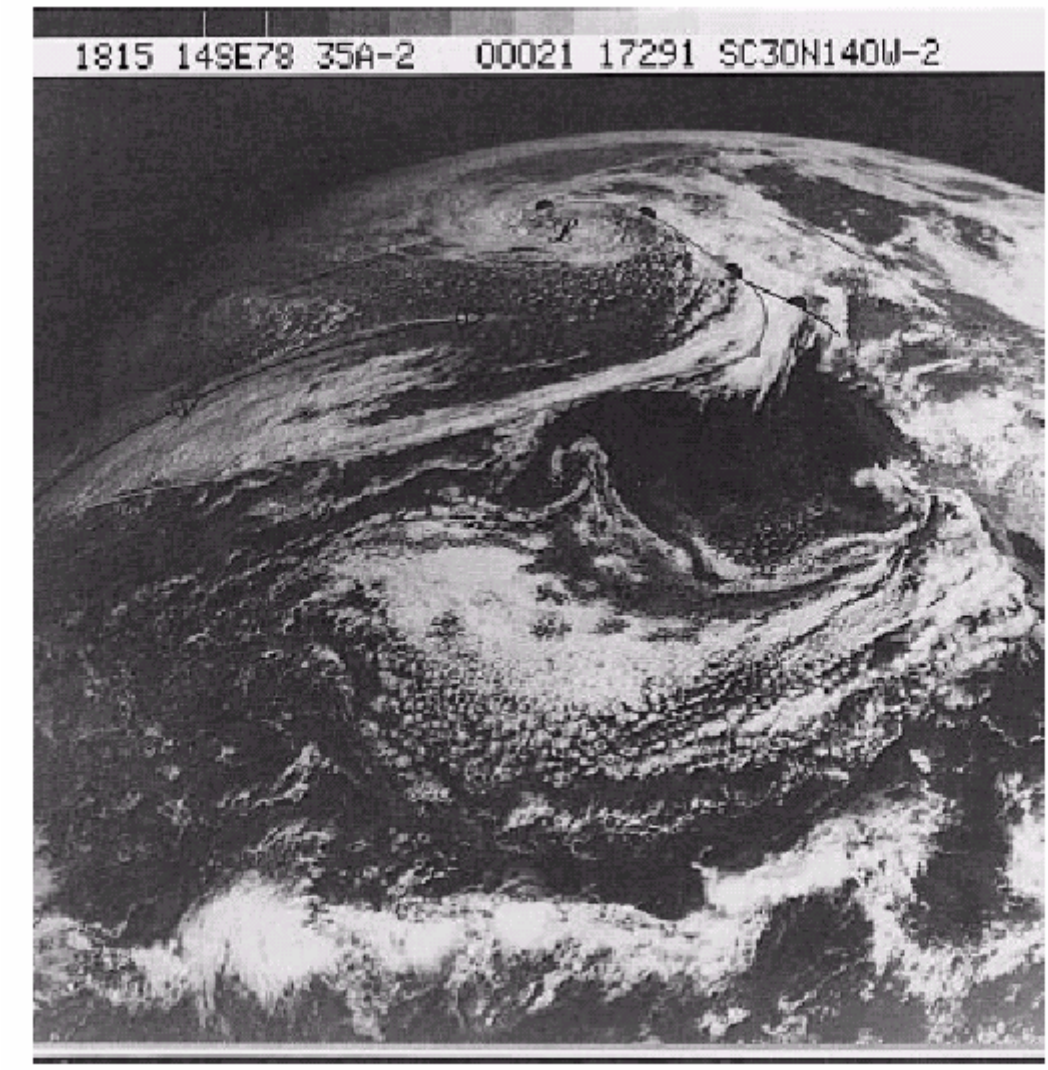

FIG. 7. Visible satellite cloud image for the northern Pacific at the time of Fig. 6.

Fig. 2.12. Visible band view of the atmospheric cyclone.

RADARSAT SAR image of the polar cyclone together with surface pressure analysis is shown on Fig. 2.13.

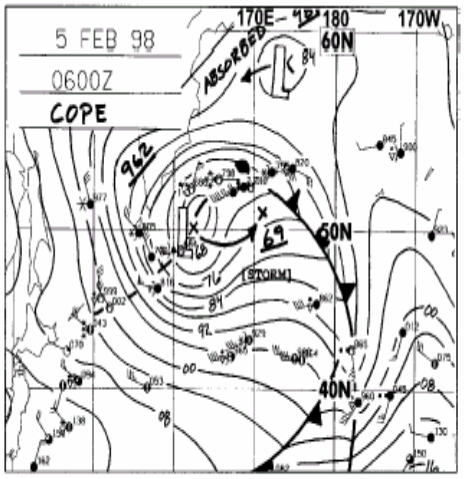

FIG. 4. MPC surface analysis for 0600 UTC 5 Feb 1998. Contour interval for isobars is 4 hPa.

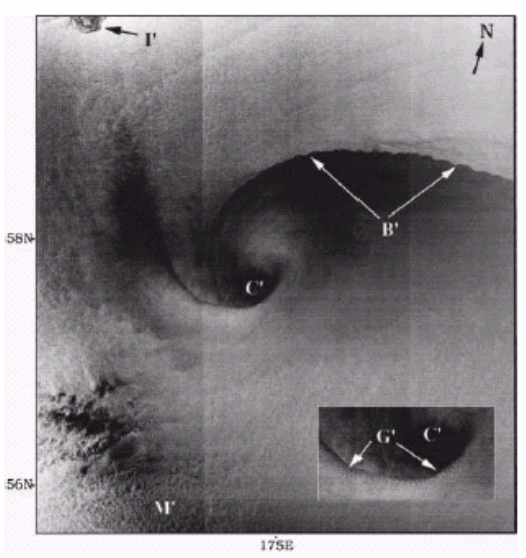

FIG. 5. RADARSAT SAR image from 0602 UTC 5 February 1998. Letters refer to features discussed in text. Copyright Canadian Space Agency (CSA) 1998.

Fig. 2.13. Pressure analysis (left) and RADARSAT SAR image (right)

Center of cyclone is labeled C.' B' is a wind direction and wind speed shear boundary. It is associated with the cloud signature and therefore lies along a frontal zone associated with the PMC.

At the center of the PMC is an isolated area of low backscatter or low wind speed. Areas of low wind speed at the center of PMCs coincides with warm cores PMC resulting from warm air seclusion as cold air wraps around the PMC.

Close inspection of image reveals mesoscale and microscale structure in and around the PMC. For example, wavelike features having wavelengths of about 20 km are seen along B'. Horizontal wind shear instability may be responsible for their occurrence.

Other finescale structure shown in image includes the presence of alternating fingers of high and low backscatter along the southern edge of the PMC's center (labeled G' in the inset). These fingers, which have a wavelength of about 2 km, bear a strong resemblance to the SAR signature of atmospheric gravity waves. The mottled backscatter appearance to the southwestern corner of the image (labeled M') is the SAR signature of cellular convection. This convection is occurring in a region of cold advection to the southwest of the PMC. Finally, the ice edge is seen protruding into the northwestern corner of the image (labeled I').

Internal waves in SAR imagery

The SAR imagery also demonstrates the manifestation on the sea surface of such processes, which are hidden in the deep sea, as internal waves. Those waves displace the permanent or seasonal pycnocline inducing vertical movement of the fluid and convergency or divergency of horizontal currents on the sea surface. The variable surface currents modulate the steepness of surface waves and the intensity of the SAR signal. Therefore the front of the internal

wave could be seen on the SAR image. Fig. 2.14 shows an example of the internal waves observation by the SAR from the ERS-1 spacecraft.

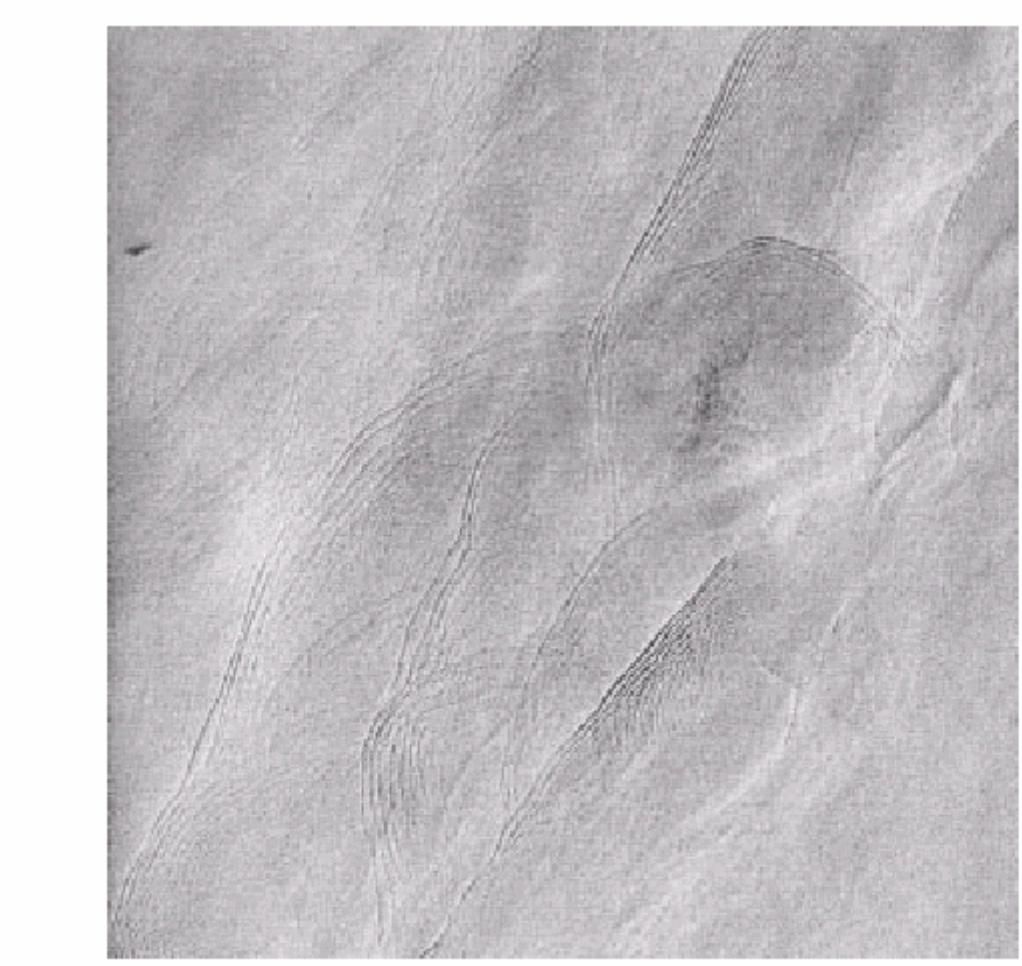

FIG. 3. *ERS-1* SAR image from 18 July 1992 that is a 100 km × 100 km square. Note that the four strong packets of internal waves are clearly seen in the lower center of the image.

Fig. 2.14. Internal waves manifecstation in the SAR imge.

Observation of sea ice in real aperture radar image.

Difference in scattering properties of open water and ice or ice covered by snow permit to observe ice sheets evolution in radar imagery (Fig. 2.15)

Thus examples of the analysis of the scanning imagery of the ocean from space show that the new quality of scanners, namely broad and repeating overview of the large oceanic areas, provides efficient tool for observation of many oceanic phenomena and study of their dynamics. Joint use of different instruments permit to characterize some processes in their complexity and to establish interdisciplinary links The scanning imagery permit to interpret much more accurately *in situ* data providing a supporting information about the background state of the basin.

Sych-1 # 2615 24 February 1996

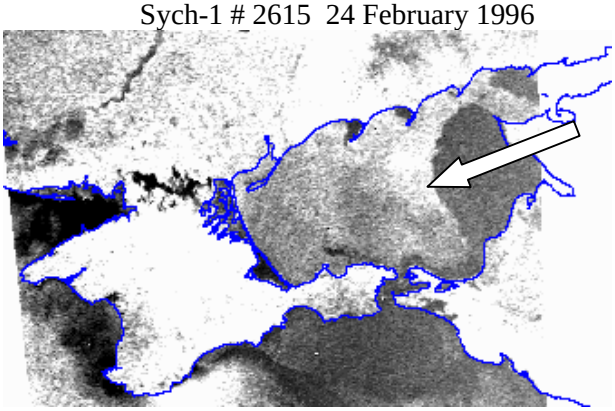

Sych-1 # 2776 06 March 1996

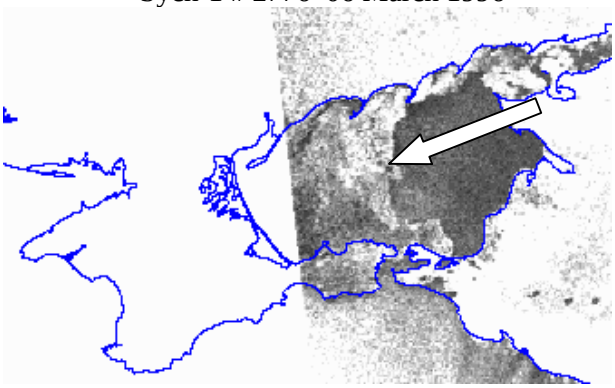

Sych-1 # 3406 18 April 1996

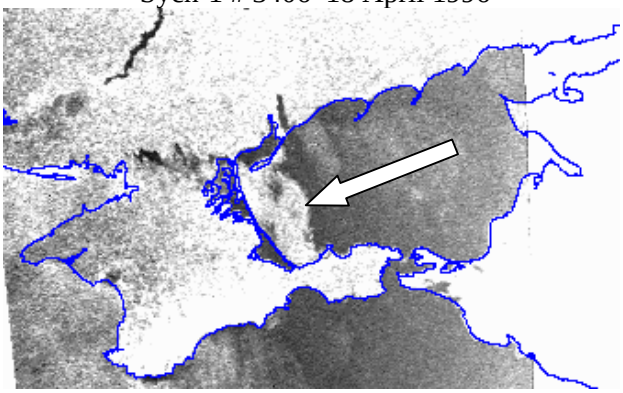

Fig. 2.15. Evolution of the ice sheet observed by the Sych radar.

3.SIGNIFICANCE OF REMOTE SENSING FOR THE OCEANIC MODELS

3.1 MULTI-CHANNEL SYSTEMS AS A MEANS OF MEASUREMENTS FROM SPACE

Observations of the ocean from space provide qualitative description of many oceanic phenomena and processes. However practical issues demand quantitative characterization of oceanic fields for nowcasting and forecasting of its state. Therefore the development of instruments, methods and algorithms, which are capable to provide quantitative measurements from space, is one of the major tasks of the ocean remote sensing. We have discussed above that

the typical situation of the remote sensing is that the radiation on each wavelength depends from the set of atmospheric and oceanic parameters. A careful investigation of the formation and transport of the radiation makes possible to select such wavelengths where dominates the input of the parameter which we like to measure. Then we can use observations on another wavelengths to correct the measurement of the basic channel and to achieve the relevant accuracy. Thus, the problem of measurements from space is solved by means of the use multi-channel systems. This principle is applied for all measurements from space available now.

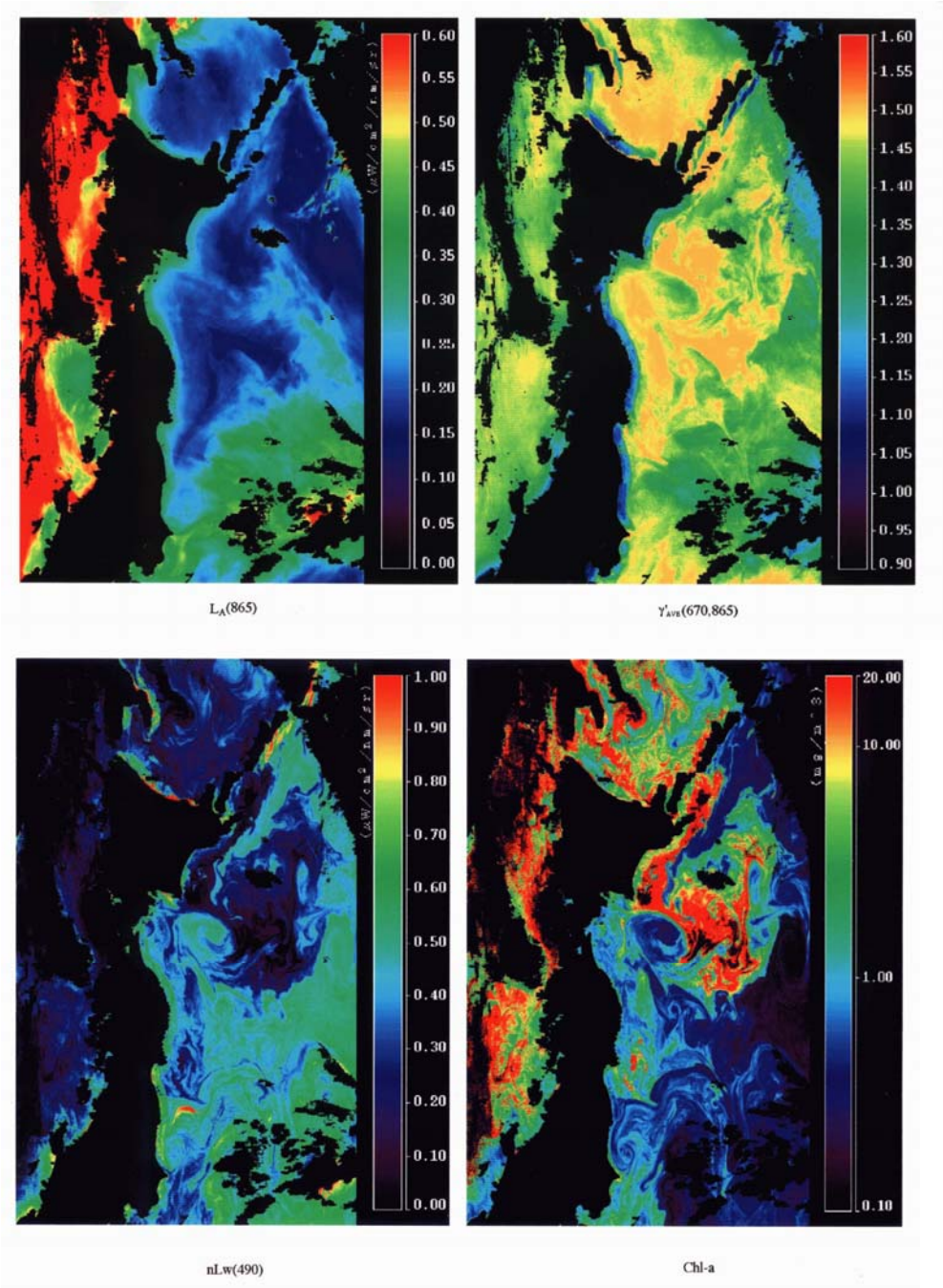

Fig.3.1. Observations of atmospheric scattering (top left) permits to evaluate the Angstrem degree (top right), then to correct atmospheric effects, obtain the water leaving radiance on the sea surface (bottom left) and finally the chlorophyll *a* concentration (bottom right).

Atmospheric correction in visible band spectrometry

The major final product of the visible band multi-channel measurements is the chlorophyll concentration, direct characteristic of the low level trophic chain of the marine ecosystem. The absorption of light by the chlorophyll pigments determines the color of the ocean. Therefore the spectral reflectance of the ocean depends from the concentration of chlorophyll. This dependence is used for estimation of the chlorophyll concentration from remote measurements.

However direct measurements of the spectral reflectance impossible due to the scattering of the light in the atmosphere. The scattering in the atmosphere is produced by molecules and by aerosols. The scattering by molecules is estimated from the theory while aerosols (more exactly, aerosol optical thickness) should be found from remote measurements.

Now it is developed the algorithm, which is based on the estimation of the aerosol optical thickness from the near infrared band measurements and its extrapolation to the visible light. The knowledge of the aerosol optical thickness gives possible to evaluate the atmosphere transparency in visible band and to remove atmospheric influence. Then the concentration of chlorophyll is estimated based on the empirical correlation with the spectral irradiance. The sequence of appropriate steps is presented on Fig. 3.1 for the atmospheric correction of OCTS observation and evaluation of chlorophyll content near the shore of Japan.

The algorithm described above with some modification is used for the regular mapping of the chlorophyll field over the whole World Ocean. The composite maps are used for filling gaps on each image conditioned by clouds. An example of the monthly averaging composite map is presented on Fig. 3.2 where major features of the global distribution of the chlorophyll in the ocean are well seen.

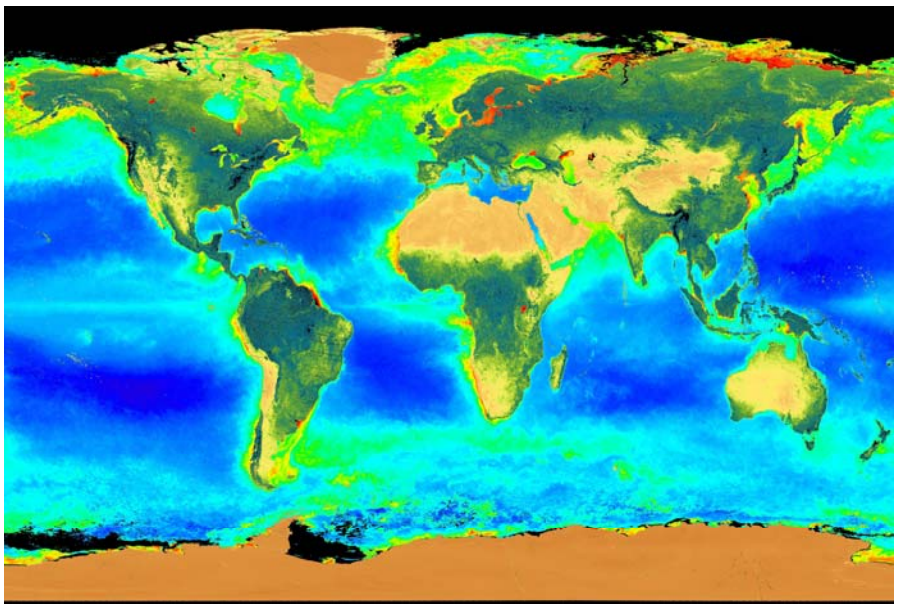

Fig. 3.2. Global chlorophyll distribution derived from space observations.

The chlorophyll determines the spectral reflectance of the open-sea waters (so called Case 1 water). The water near the shore (Case 2 water) is more turbid and the light is scattered additionally by suspended particles. Therefore the univocal correspondence between the spectral reflectance of the sea and chlorophyll is destroyed. Accurate separation of terrigenic particles and biogenic materials in Case 2 water is the complicated problem. The complexity of the problem is demonstrated by Fig. 3.3 where one could find the difference between sediments and algae bloom.

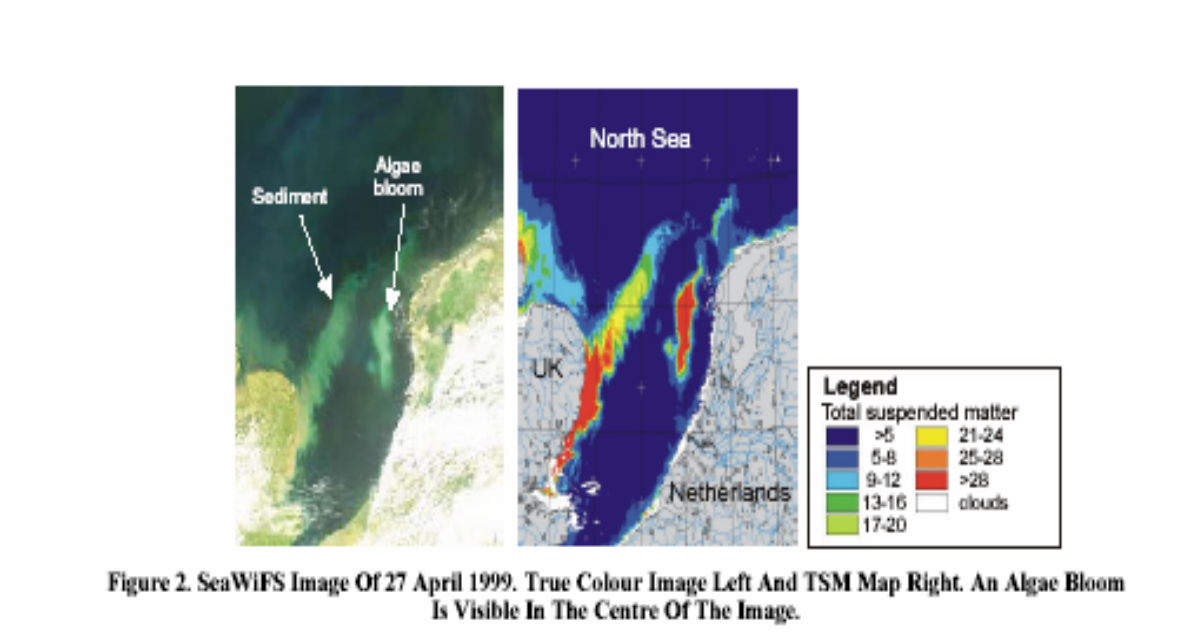

Figure 2. SeaWiFS Image Of 27 April 1999. True Colour Image Left And TSM Map Right. An Algae Bloom Is Visible In The Centre Of The Image.

Fig. 3.3. The difference of sediments and algae bloom observations.

Atmospheric correction of IR observations

The emissivity coefficient of the water could be considered as a constant in the thermal IR diapason. Therefore the sea surface temperature (SST) determines the radiance emitted by the sea surface. However the absorption in the atmosphere (mainly by the water vapor), the radiance emitted by the atmosphere directly upward and reflected from the sea surface contaminate the signal received on the satellite. Fortunately the contaminated factors could be removed by means of the simple two or three-channel linear algorithm

$$T_S = 1.0574 \cdot T_{3.7} + 0.447 \cdot (T_{3.7} - T_{10.5}) - 14.4$$

or

$$T_S = 1.035 \cdot T_{10.5} + 3.046 \cdot (T_{10.5} - T_{12}) - 10.78$$

where SST is in the left side of the equation. The right side of the equation instead of the radiation contains so called “radiation temperature” which is connected with radiation by the Plank formula. The index in the right side of the equation shows the channel wavelength. Measurements are carried out in the transparency windows where the atmospheric influence is

rather low. Final accuracy of the SST determination using linear algorithms is about 0.5 degree. Clouds produce some restrictions to the mapping of SST using IR radiometry. A map of SST reconstructed based on one day measurements contain lot of gaps, which could be filled by means of spatial averaging or by means of data collection for some days and construction of composite SST maps. An example of global SST map obtained from one-day survey is presented on Fig. 3.4.

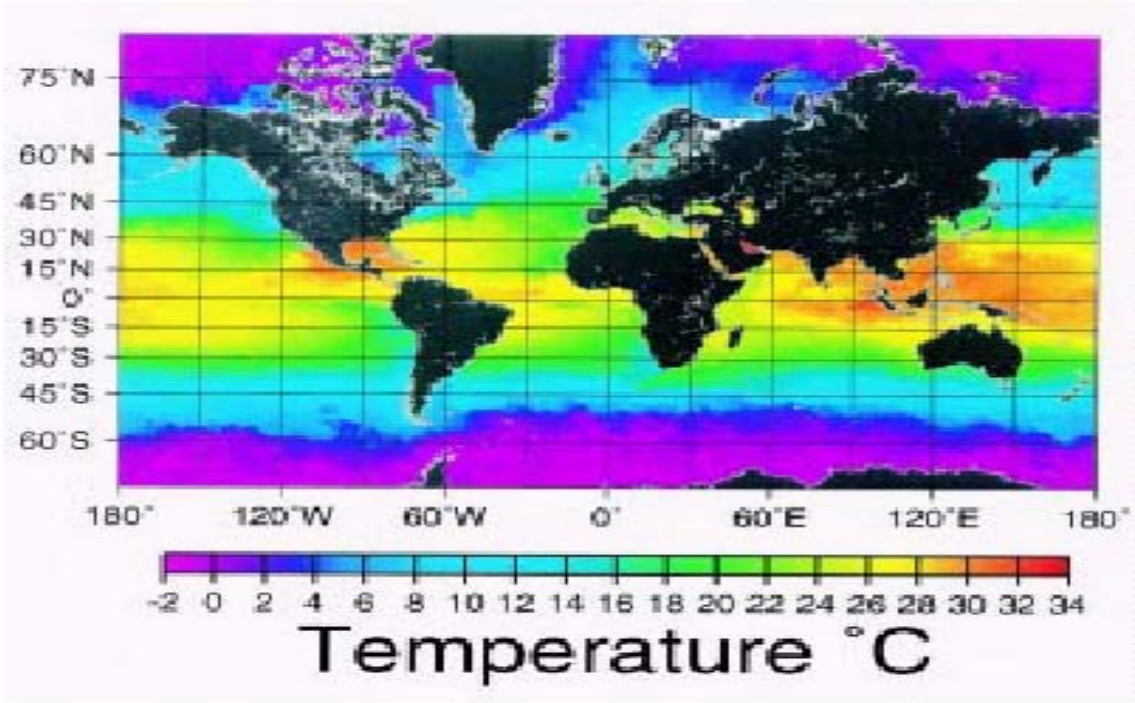

FIG. 4. Global 100-km satellite SST analysis from 23 July 1996.

Multi-parametric problem of microwave radiometry

Radio-frequencies have the advantage before visible and IR bands as even a cloudy atmosphere is almost transparent in this range. Nevertheless the total water vapor content and water content in clouds should be taken into consideration for accurate estimation of the sea surface state. The emissivity coefficient of the sea surface depends from surface temperature, salinity (for decimetric waves) and foam coverage, connected with the near surface wind. Therefore the sea surface temperature, sea surface wind and sea surface salinity could be found from the multi-channel remote sensing data in microwaves. An example of the monthly map of sea surface wind from microwave radiometer together with climatologic fields is presented on Fig. 3.5. Maps manifest good consistency demonstrating the quality of the remote sensing data.

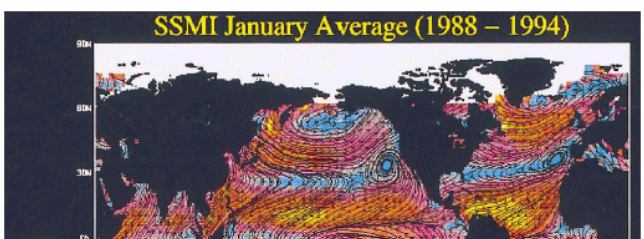

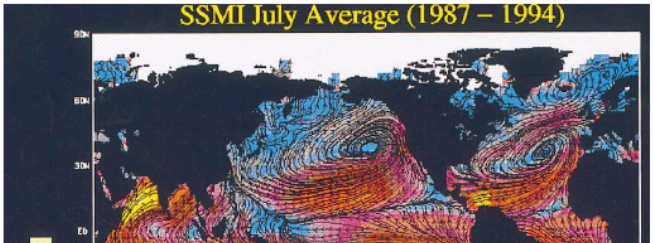

Wind determ

The sea surface salinity measurements from space are not available now. However the set of encouraging experiments is carried out using planes. Fig. 3.6 shows results of one of experiments where is evident good correspondence of salinity measurements from the aircraft and *in situ* data. Therefore it is possible to hope that the routine salinity measurements soon will be available for the oceanographic community.

Fig. 3.5. Wind observation by the microwave radiometer.

dec n the use of centimetric and

cen ce. Now it is about ten km for

cou le features of SST field, which

dec ents are based on the use of

n.

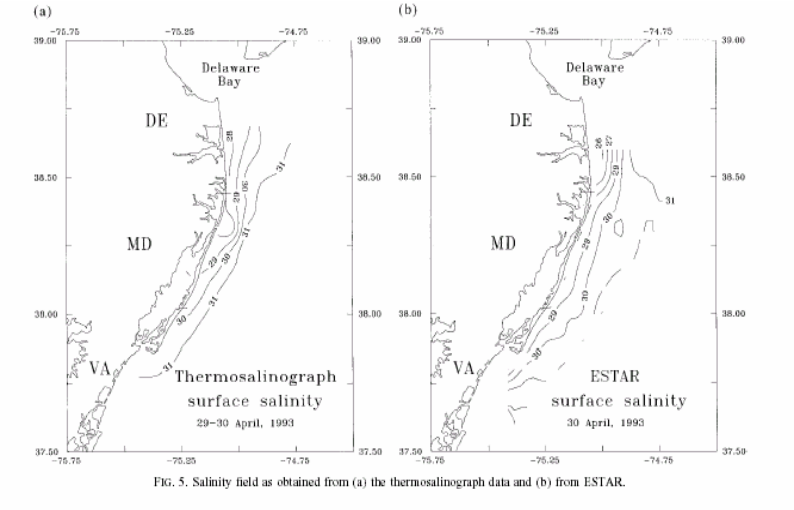

FIG. 5. Salinity field as obtained from (a) the thermosalinograph data and (b) from ESTAR.

Fig. 3.6. Surface salinity observations from aircraft (right) and from the ship (left)

Scatterometric three beam system

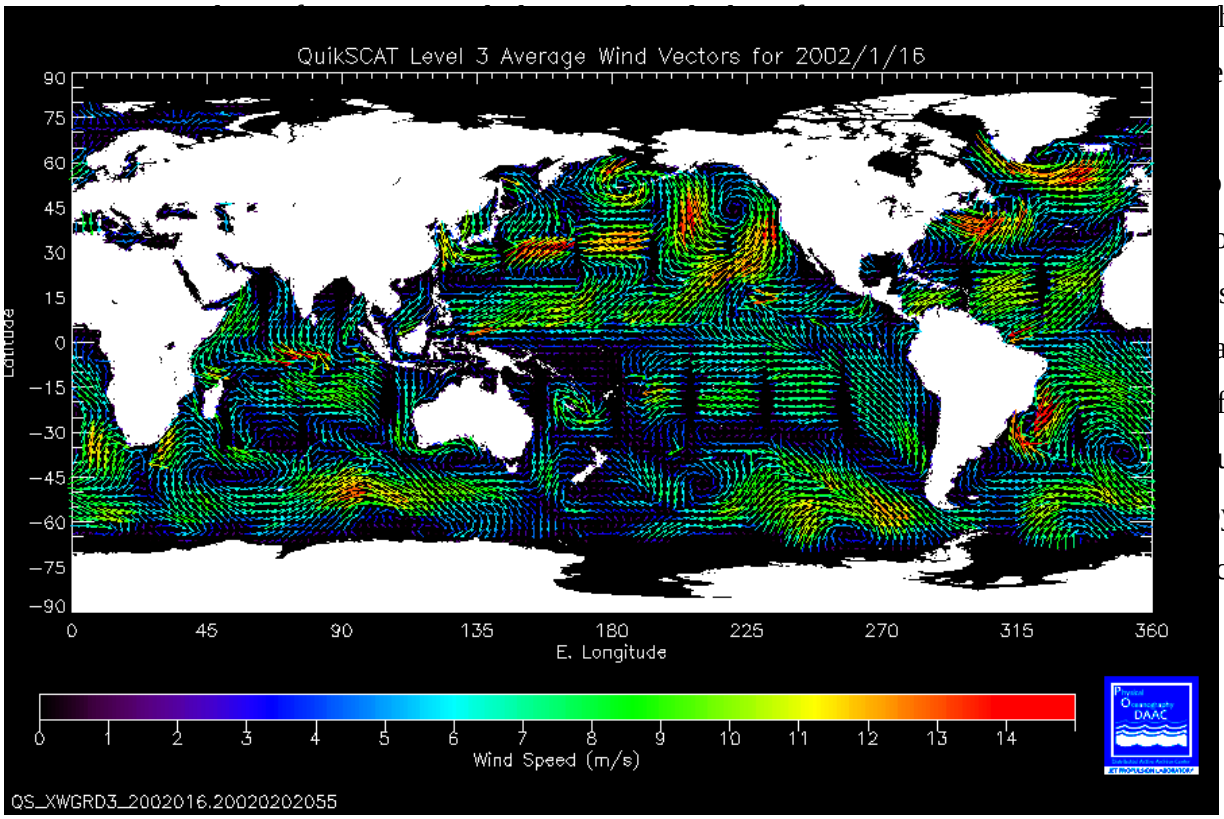

he surface
s we get
along the
the wind
the wind
surements
agram and
f the near
uity in the
y systems
curate. An

Accurate altimetric measurements

Space altimeter is one of unique devices of the ocean remote sensing. It measures the distance from satellite to the ocean surface from the height about 1200km with instrumental accuracy two cm. The set of corrections should be applied (see Table) to evaluate the distance from the satellite to the sea surface. Unfortunately absolute determination of the real surface of the ocean is impossible now due to the low accuracy of the geoid knowledge. However the anomaly of the sea surface elevation could be estimated from the space altimeter measurements with the rms accuracy 4cm. This accuracy permits to measure tides and the sea level oscillations in semi-enclosed basins.

Source of Error	Uncorrected (Seasat) (cm)	Corrected (Seasat) (cm)	Corrected (Topex) (cm)	Wavelength (km)
Geoid	100(m)	100-200	10-50	200-40,000
Orbits	5 (km)	100-200	5-10	10,000
Coordinate system	100-200	100-200	10	10,000
Ionosphere	0.2-20	0.2-5	1.3	20-10,000
Mass of air	230	0.7	0.7	1000
Water vapor	6-30	2.0	1.2	50-1000
Electromagnetic bias*	4	2	2.0	100-1000

However the major advantage of the altimeter measurements is connected with the mapping of the sea surface elevation. The sea level gradient on low frequencies characterizes so called gradient currents. Gradient currents are determined by the geostrophic relation everywhere except for the narrow band near the equator. The geostrophic relation connects the slope of the sea level and surface gradient currents according to formula:

$$-f \cdot v = g \cdot \frac{\partial \varsigma}{\partial x} \qquad f \cdot u = g \cdot \frac{\partial \varsigma}{\partial y}$$

where u, v are components of the current velocity, f is the parameter of Coriolis, g is the gravity and ς is the level of the sea. The sea surface level corresponds to the dynamic topography on the sea surface and Fig. 3.8 shows how altimeter measurements reproduce major oceanic gyres simulated by the numerical model.

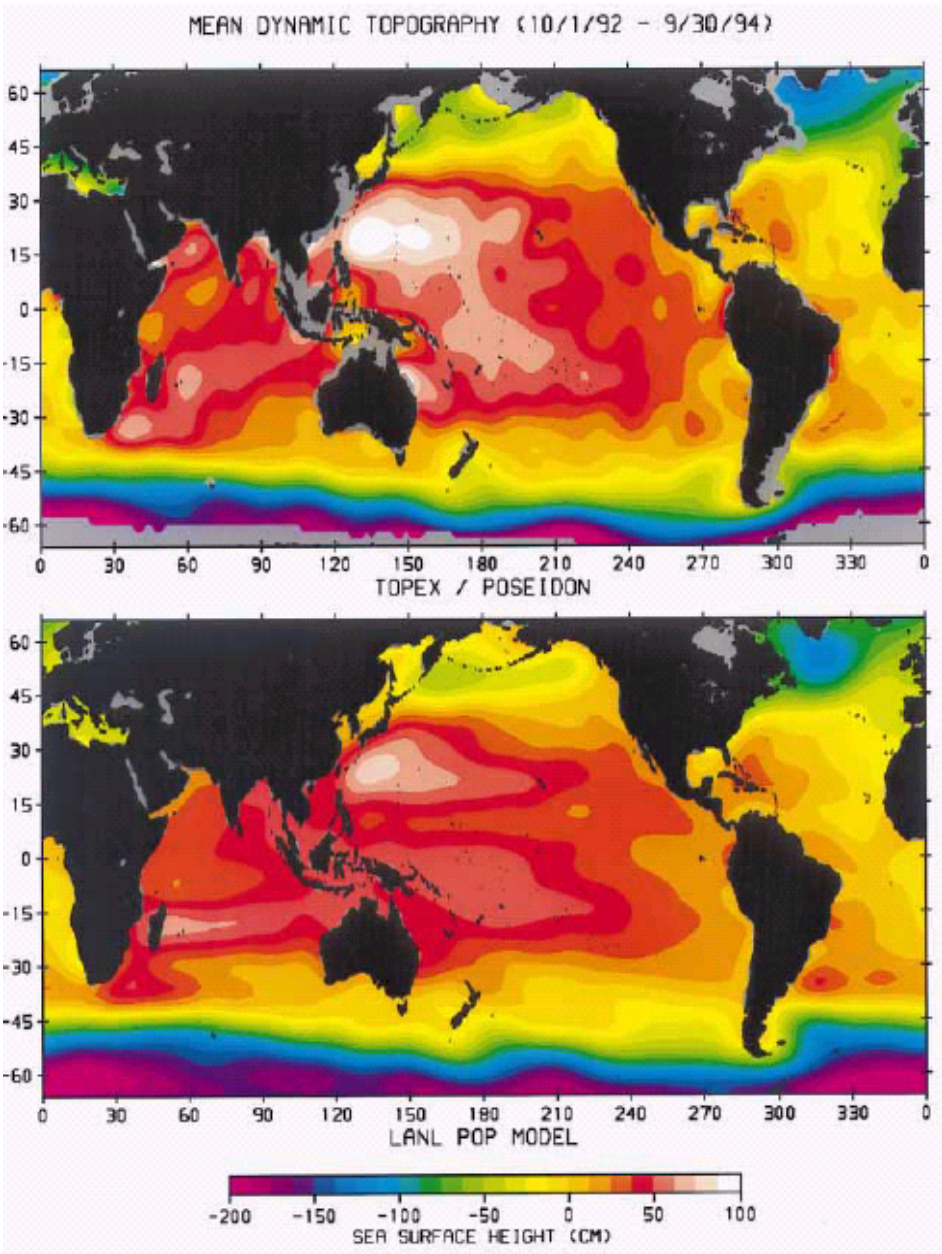

Fig. 3.9. Sea surface topography derived from altimeter measurements (top) and simulated by the circulation model.

It is known from the application of the dynamic method that

$$\zeta \approx \frac{1}{\rho_0}\int_{-D}^{0} \rho \cdot dz$$ Therefore the sea level reflects the deep-ocean processes, particularly mesoscale eddies, meanders of currents, planetary waves. Long-term averaging of the root-mean-square sea surface elevation reflects the spatial distribution of energy of mesoscales. Fig. 3.10 shows the correspondence of altimeter measurements and simulations by the eddy-resolving model. It is obvious that the highest intensity of mesoscales is observed near the intense currents like the Gulf Stream and Kuroshio.

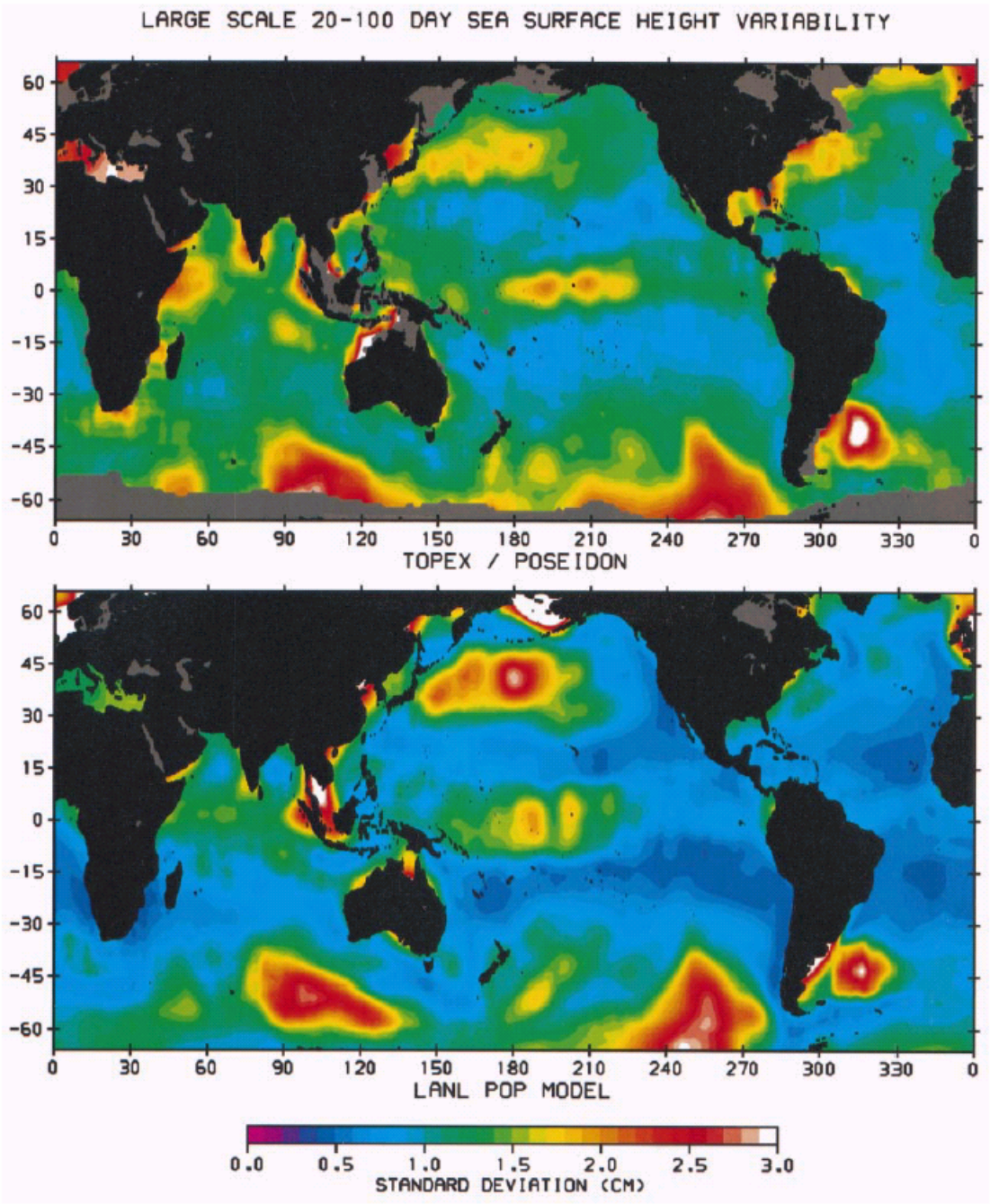

FIG. 1. Root-mean-square variability of sea surface height measured by T/P (top) and simulated by the POP ocean general circulation model (bottom). Both were filtered to retain energy at spatial scales larger than 1000 km and temporal scales from 20 to 100 days. [From Fu and Smith (1996).]

Fig. 3.10. Rms variability of the sea surface height measured by altimeter (top) and simulated by the circulation model (bottom).

3.2. APPLICATION OF THE REMOTE SENSING TO THE MODELING OF OCEANIC DYNAMICS

Remote sensing measurements provide unique possibility for the near real time application of the global ocean circulation models as they supply practically all boundary conditions on the ocean surface. Scatterometer or passive microwave radiometer are sources of

the momentum fluxes on the sea surface, major driving force of the oceanic circulation. Temperature and salinity measurements from space specify thermodynamic boundary conditions for the global circulation models. Altimeter data characterize in integral form large-scale and mesoscale processes occurring in the deep-ocean and assimilation of the altimeter measurements permit to reduce the model uncertainties in simulation of realistic circulation.

Application satellites as the data transmission system permit to use additional information about the sea state. Among others the most important seems the use of the profiling buoys which could be launched at some depth and propagate there transporting by currents. A buoy rises to the surface over the prescribed period of time and measure temperature and salinity profiles which then transmitted through the satellite. Then a buoy sinks again to the initial depth and the cycling repeats. The remote sensing data together with the use of satellites as data transmission system provide following data sets for the global circulation models (see Table).

Boundary conditions	*Deep-sea characteristics*
Sea Surface Temperature **Sea Surface Salinity** **Wind Stress** **Short wave radiation**	**Altimetry** **Temperature and salinity profiles**

Using realistic boundary conditions and assimilating deep-sea data models are capable to reproduce continuous monitoring of currents and deep-sea hydrography. Fields obtained after assimilation provides good model initialization for the following forecast of the basin dynamics

MORE REFERENCES

There are plenty of books where the introduction to the ocean remote sensing is presented. The reference to couple of them is given below.

Stewart R. Methods of Satellite oceanography. Univ. of California Press 1985

Seelye Martin An Introduction to Ocean Remote Sensing

University of Washington

Hardback

An Introduction to Ocean Remote Sensing describes the use of satellite data in the retrieval of oceanic physical and biological properties. It gives examples of the kinds of data that can be acquired and describes their oceanographic application. It also describes the national and international programs in satellite oceanography that have been initiated during the past two decades, and reviews current and future programs up to 2019. The book covers radiative transfer,

ocean surface properties, satellite orbits, instruments and methods, visible remote sensing of biological properties, infrared sea surface temperature retrieval, passive microwave measurements, scatterometer wind retrieval, altimetry and SAR. New and proposed techniques, such as polarimetric passive microwave radiometers and SARs, interferometric radar altimetry and sea surface salinity retrieval are also discussed. This textbook is designed for graduate and senior undergraduate courses in satellite oceanography, and will prepare students and interested scientists to use satellite data in oceanographic research.

• It gives a unified treatment of the principles of satellite instruments and their application
• It covers a broad range of instruments and principles of operation
• It describes the past and present of ocean remote sensing and summarizes potential future instruments and programs up to 2019

Contents

Preface; 1. Background; 2. Ocean surface phenomena; 3. Electromagnetic radiation; 4. Atmospheric properties and radiative transfer; 5. Reflection, transmission and absorption at the atmosphere/ocean interface; 6. Ocean color; 7. Infrared observations of sea surface temperature (SST); 8. Introduction to microwave imagers; 9. Passive microwave observations of the atmosphere and ocean surface; 10. Introduction to radars; 11. Scatterometer observations; 12. The altimeter; 13. Imaging radars; 14. Future oceanographic satellite systems: 2003 to 2019; Appendix 1; Appendix 2; References; Index.

Some additional information about the ocean remote sensing could be found at:
http://ioc.unesco.org/oceanteacher/OceanTeacher2/01_GlobOcToday/01_SciOc/05_RemSens/REmoteSensing.htm

3.1.1.1.2. Surface drifting floats

One of the efficient tool of operational oceanography is surface drifting buoy (drifter). That buoys free drifting on the sea surface and measuring current velocity on the depth 12-15 meter where they have a sail. The position of drifters is determined by the stallite ARGOS system. Additional sensors could be on the buoy to measure SST, pressure, water transparency, etc. Data of measurements are transmitted by the same satellite to the processing centers in the real time. The shape of the buoy is seen on Fig. 1.

Fig. 1. Launch of the drifter.

More than thousand of buoys are launched now in the World Ocean (Fig.2). Observations by drifters allow map surface currents (Fig. 3)

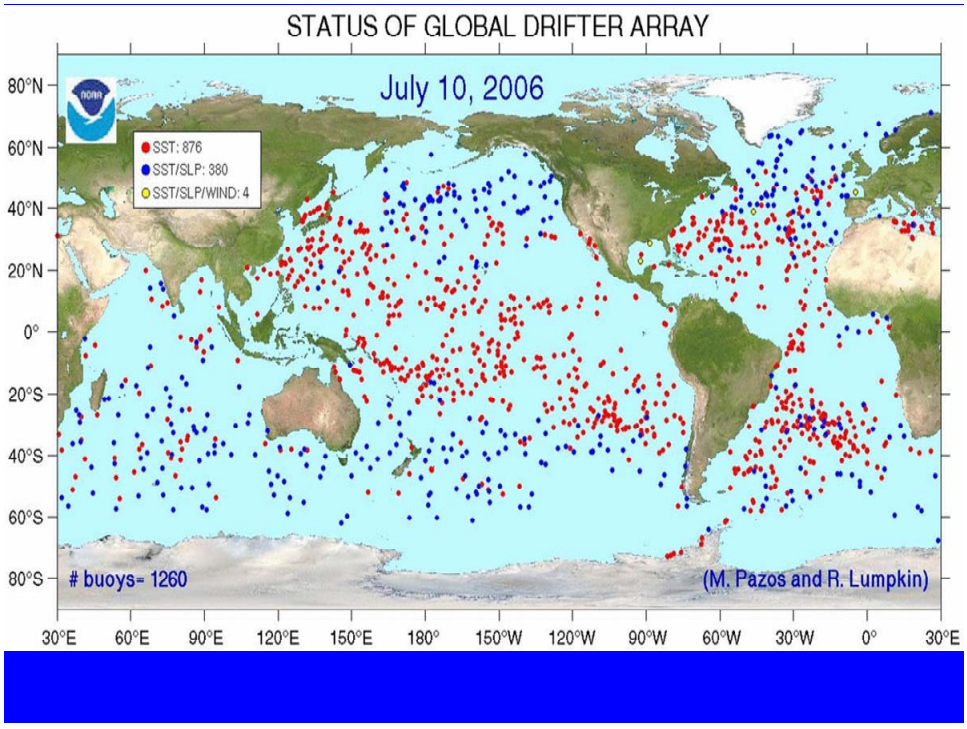

Fig. 2. Global drifter array

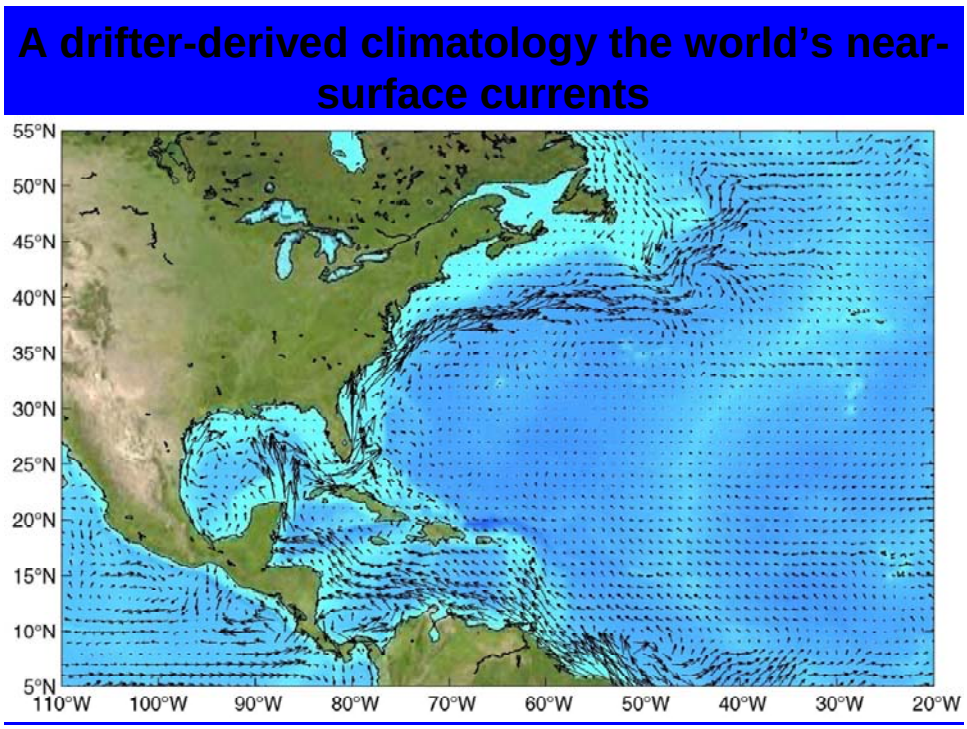

Fig. 3. Surface currents map derived from observations by drifters.

Drifters could have the termister chain (Fig. 4) measuring the temperature variability in the upper layer of the ocean. Example of the upper layer temperature observations in the Black Sea is presentd on Fig. 5.

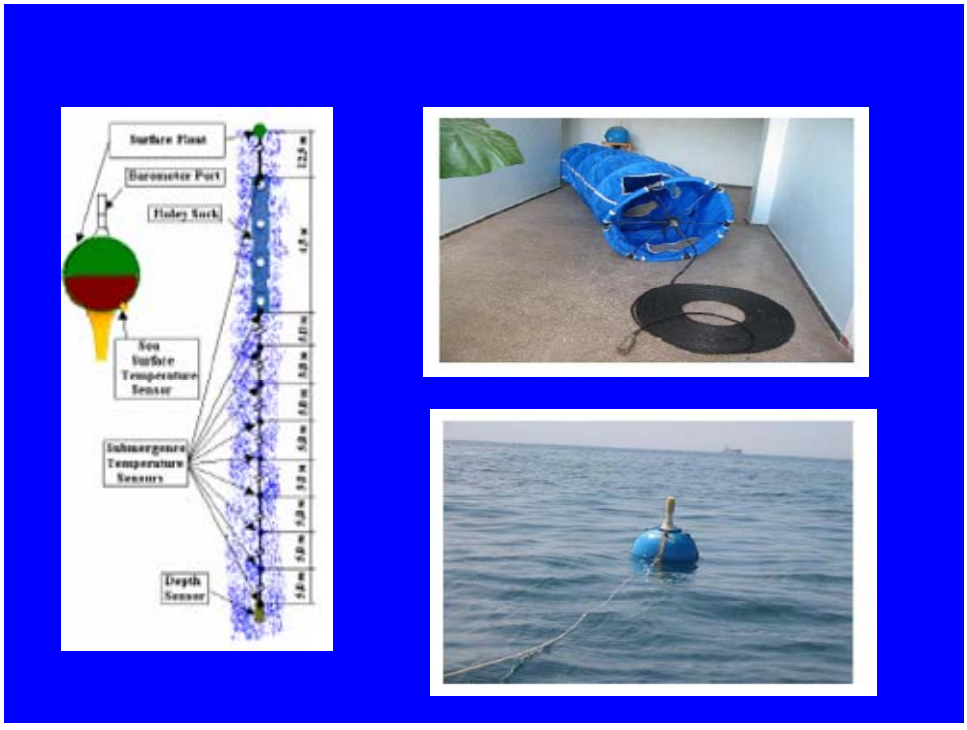

Fig. 4. Drifting buoy with termistor chain.

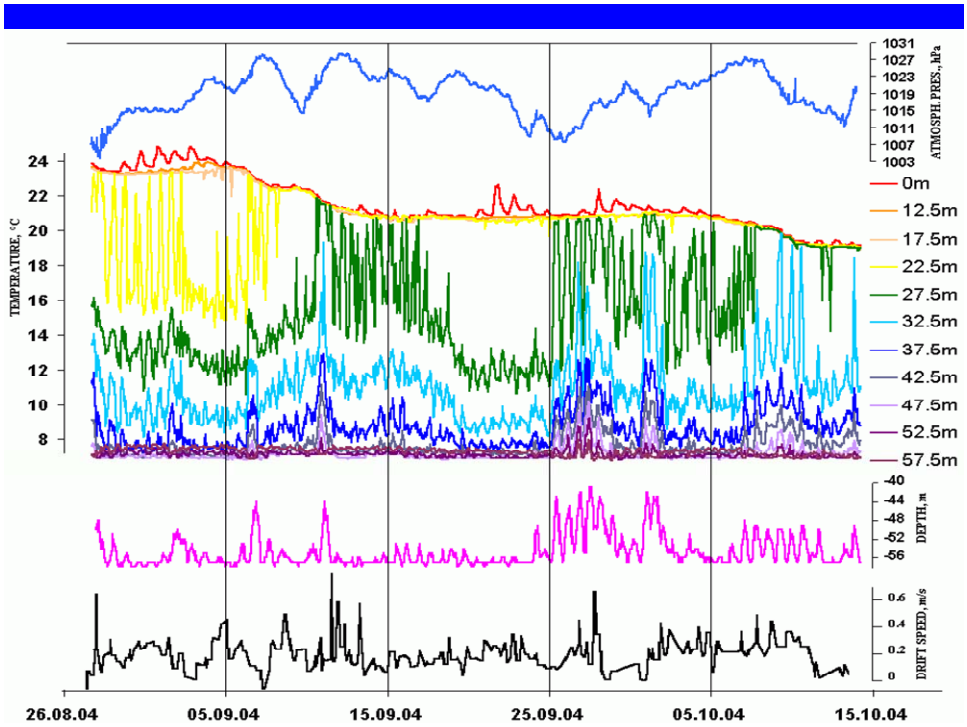

Fig. 5. High frequency variability of temperature in the upper layer of the Black Sea.

More information about drifting buoy measurements could be found at

http://www.aoml.noaa.gov/phod/dac/gdp_information.html

3.1.1.1.3. Profiling floats

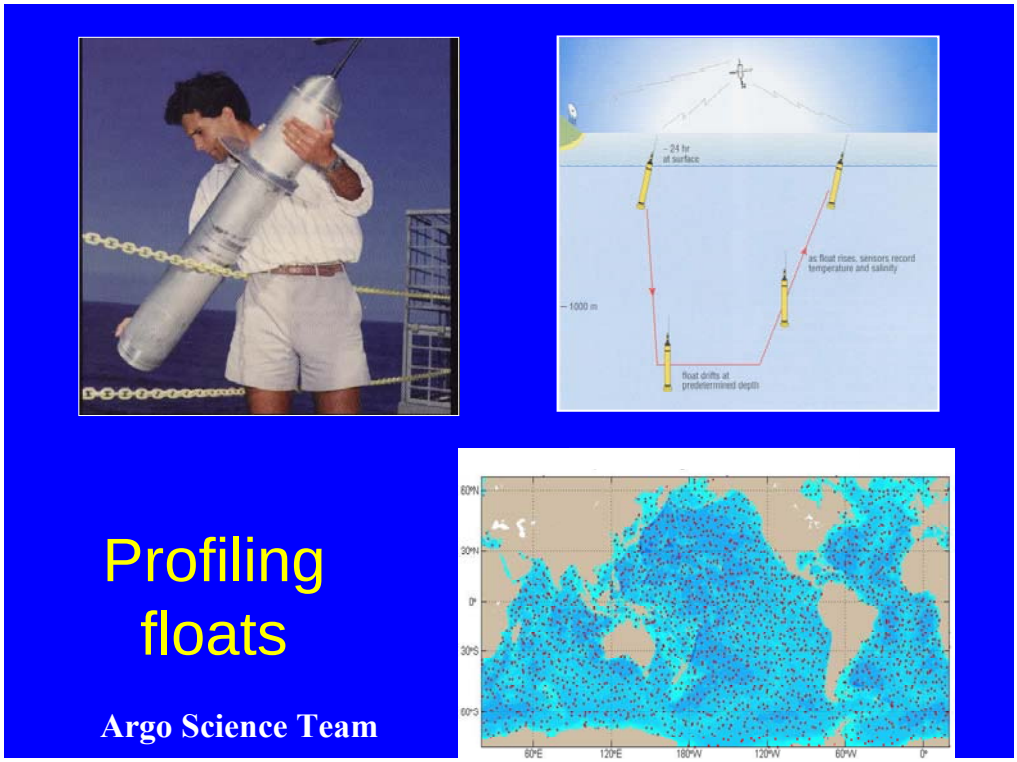

Fig. 1. The view of the profiling float (top left), the measuring cycle of the float (top left) and the array of profiling floats at the World Ocean (bottom left)

Another very efficient tool of operational oceanography is profiling float. It sinks to the prescribed depth after the launch at sea and freely transported by currents during the prescribed period of time (usually one week – ten days). After that time the float changes its buoyancy and rises to the sea surface profiling temperature and salinity. Its position after rising to the surface is determined by the satellite and measurements of temperature and salinity are transmitted through the satellite to the processing centers. Examples of temperature and salinity profiles obtained at the Black Sea are presented on Fig. 2.

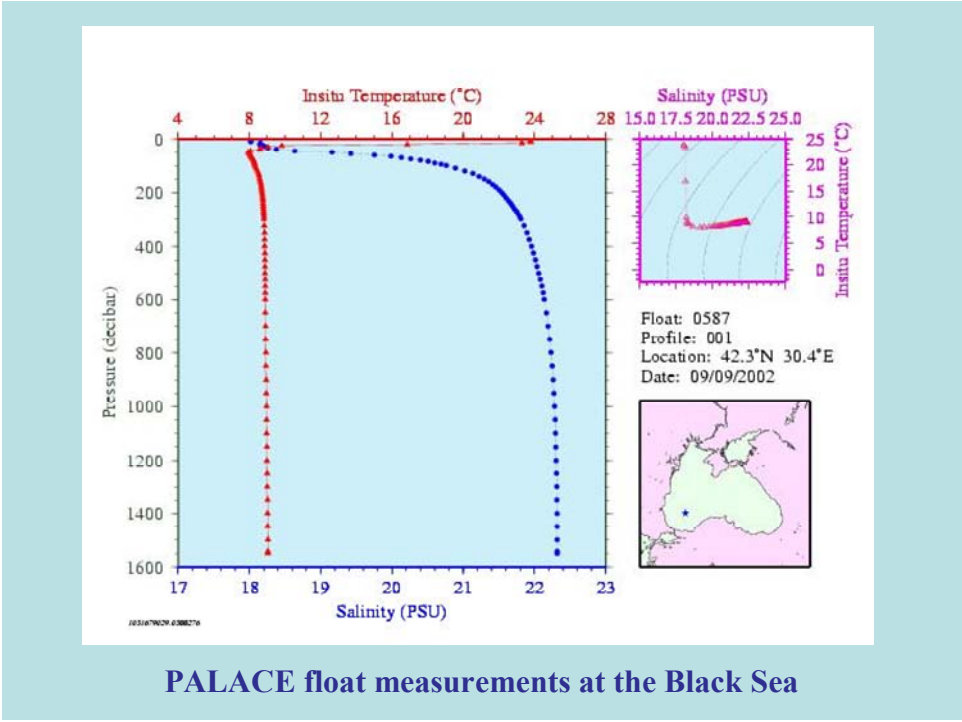

Fig. 3. Profiles of temperature and salinity obtained by a profiling float at the Black Sea.

More information about profiling float measurements could be found at:
http://www-argo.ucsd.edu/index.html

3.1.1.1.4. Ships of opportunity

The primary goal of the Ship-of-Opportunity Programme (SOOP) is to fulfill upper ocean data requirements which have been established by GOOS and GCOS, and which can be met at present by measurements from ships of opportunity (SOO). SOOPIP is establishing itself as an operational programme and is therefore participating in the Joint WMO-IOC Technical Commission for Oceanography and Marine Meteorology (JCOMM) and particularly in its Ship Observations Team (SOT). Data management is taken care of through the Global Temperature Salinity Profile Programme (GTSPP).

The SOOP is directed primarily towards the continued operational maintenance and co-ordination of the XBT ship of opportunity network but other types of measurements are being

made (e.g. TSG, XCTD, CTD, ADCP, pCO2, phytoplankton concentration). This network in itself supports many other operational needs (such as for fisheries, shipping, defense, etc.) through the provision of upper ocean data for data assimilation in models and for various other ocean analysis schemes. One of the continuing challenges is to optimally combine upper ocean thermal data collected by XBTs from the SOO with data collected from other sources such as the TAO array, Argo, and satellites (eg. AVHRR, altimeter, etc.). However, it is considered most important to have the SOOP focused on supporting climate prediction in order to ensure the continued operation of the present network.

In August 1999 an upper ocean thermal review, was conducted by OOPC, CLIVAR Upper Ocean Panel, and SOOP in order to (i) compile a consolidated account of the existing upper ocean thermal database, (ii) produce consolidated maps of information level/content based on the dominant scales of climate signals; (iii) document the existing practices for assembling, quality control and distribution of upper ocean data; (iv) document to the extent possible the "value adding" of thermal data process chains, be they automated assimilation, quick-look/semi-automated quality control or higher-level scientific quality control and assembly, (v) provide quantitative assessment of all SOOP lines including an assessment of relevance/impact against scientific objectives, (vi) provide a renovated SOOP plan taking account of, as far as is practical the existence (or potential) of other direct sampling networks (e.g., TAO, Argo), the indirect information available from remote sensing, particular altimetry; and the indirect information available from models, e.g. wind-forced equatorial.

The review noted that (see conclusions), till this point of time, sampling had been in three modes: low density, frequently repeated and high density. The SOOP has been extremely cost-effective for science and, latterly, for operational applications. However the review proposed a major revision of the ship-of-opportunity program. The program would gradually withdraw from areal sampling as Argo was implemented, and would at the same time ramp up its effort in line (transect) sampling. The line sampling would include both intermediate resolution, frequently repeated lines (see proposed FR lines) and high density (see proposed HD lines), quarterly repeat lines. This change in approach enhances complementarity with existing elements, particularly TAO and altimetry, and seeks optimum complementarity for the system envisaged for the future. The new design will address several important scientific goals, both for GOOS and CLIVAR. It will make unique contributions in terms of in situ eddy-resolving data sets and in terms of the repeated lines. It is estimated that this new design will not have significant resource implications. The review noted that this new mode of operating does open up further opportunities for observations from SOOP though this has to be balanced against the good-will being offered by the ships.

(from the site
http://www.ifremer.fr/ird/soopip/soopip_overview.html#INTRO
where more details could be found)

3.1.1.1.5. Moorings

Long-term measurement by the anchored buoys is an efficient way to obtain high resolution time series. Anchored buoys could have different modifications (see Fig. 1) and different sensors could be placed near the sea surface or along the wire that connects the buoy with the anchor. Thus, the set of parameters could be measured. Data of the anchored buoys could be transmitted in the real time through the satellite.

Fig. 1. Different type of buoys.

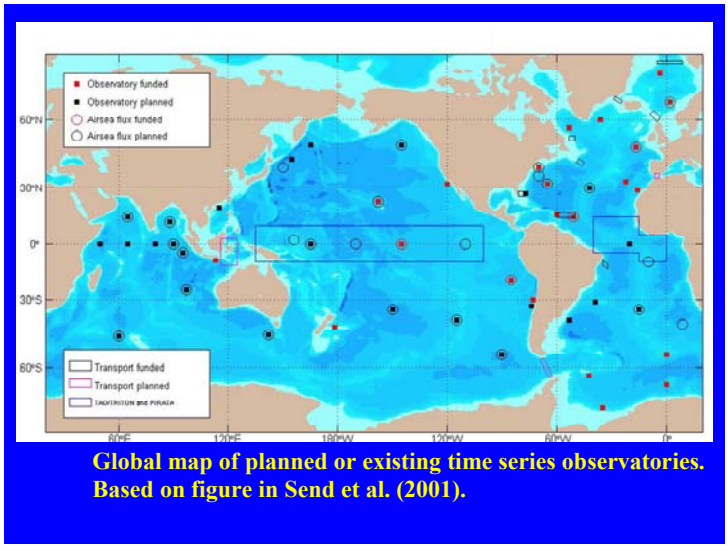

Fig. 2. Map of time series observatories.

The network of time series observations is developed now. The location of the time serie observatories is presented on Fig. 2.

More information could be found on the site

http://www.gosic.org/goos/Tropical_mooring_network_prog_overview.htm

3.1.1.1.6. Autonomous Underwater Vehicles

Autonomous underwater vehicle (AUV) is the platform which could provide autonomous measurements according to the prescribed a priori program. It may follow complicated trajectory and collect data along its path. The set of different sensors could be installed t AUV.

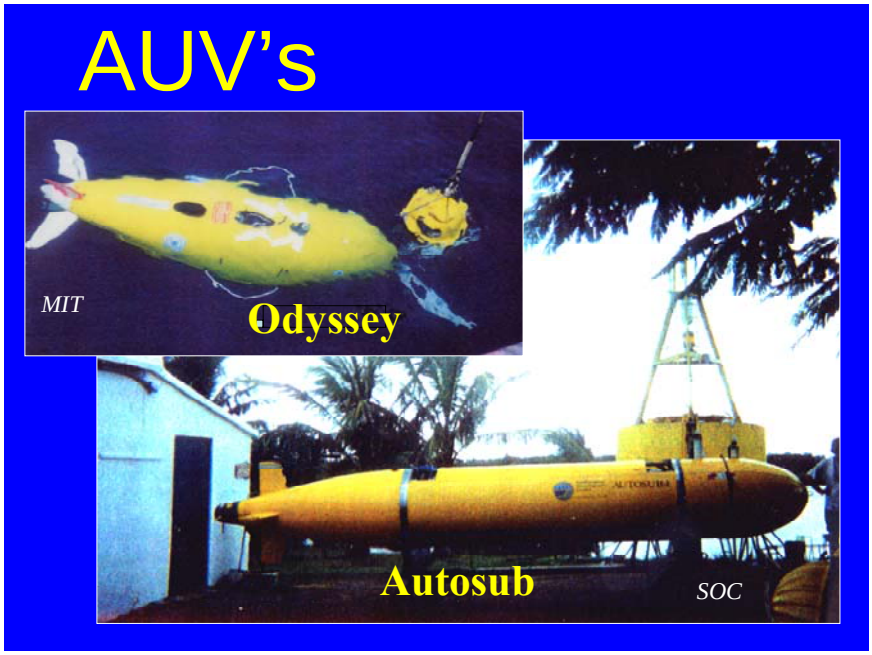

Fig. 1. Examples of AUV's.

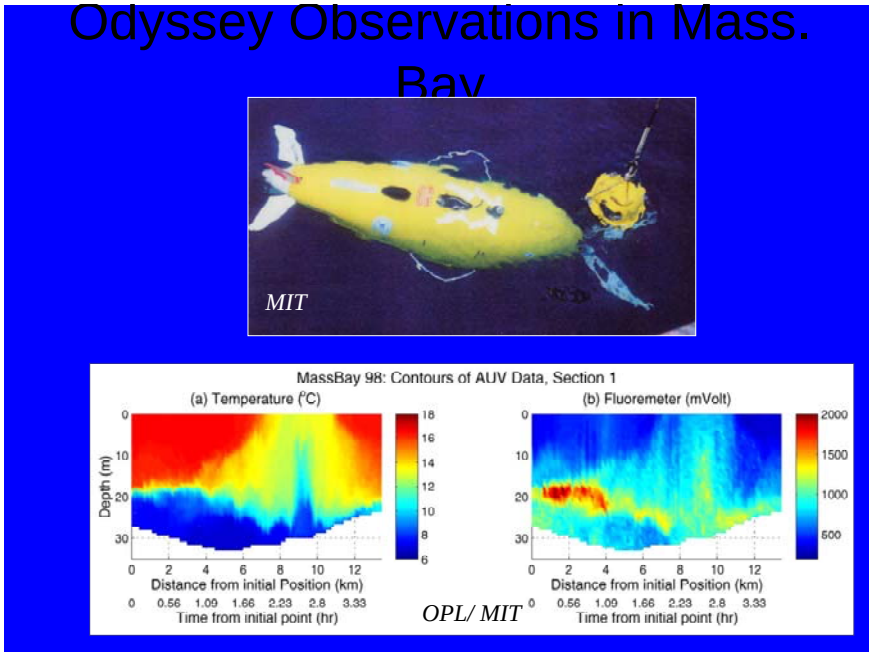

Fig. 2. Observations of temperature and fluorescence by AUV.

Examples of AUV's and observations collected by AUV's are presented on Fig. 1,2.

More information could be found at:

http://auvlab.mit.edu/

3.1.1.1.7. Sea level network

UPDATE on the status of the MedGLOSS Sea-Level Pilot Network

Dov S. Rosen

Chairman, Joint IOC/CIESM Group of Experts on MedGLOSS1. Background

Presently, a worldwide eustatic sea-level rise due to the "greenhouse effect" has been forecasted by the WMO/UNEP Intergovernmental Panel on Climate Change (IPCC). Those are due to global warming, leading to water volume expansion as the major component and ice cap melting as the secondary one. However, the report authors also recognized that regional sea-level rise may differ significantly from the globally averaged sea-level rise forecasts, in particular due to tectonic movements, meaning that relative sea-level changes may be as important or even more than those of the absolute sea-level.

Recognizing the importance of the subject for the region, as well as its capability to serve as a model for the world-wide processes, the IOC and the Commission Internationale pour l'Exploration Scientifique de la mer Mediterranee (CIESM), have agreed in 1996 to jointly cooperate in the study of this important subject by establishing a long-term monitoring network system for systematic sea-level measurements in the Mediterranean and Black Seas. The system, named MedGLOSS (Mediterranean regional subsystem of the Global Sea Level Observing System), a monitoring network system for systematic measurements in the Mediterranean and Black Seas, is being developed by applying basic GLOSS requirements and methodology, aiming to provide high-quality standardized data, which can then be directly applied for the various regional and world-wide studies.

A preliminary expert workshop on MedGLOSS was held jointly by CIESM and IOC at CIESM headquarters in Monaco in February 1996. In the summer of 1996 a Memorandum of Understanding was signed between IOC and CIESM (by Prof. Frederic Briand - Director General of CIESM, , and Dr. Gunnar Kullenberg - Secretary of IOC), establishing also a Joint Group of Experts on the MedGLOSS programme, composed of Prof. Suzanna Zerbini (Italy), Mr. Pierre-Yves Le Traon (France), Cdr. M. Emin Ayhan (Turkey) and Mr. Dov S. Rosen (Israel). Later on Dov Rosen was appointed chairman of this group. Following the recommendations of the Joint Group of Experts on MedGLOSS, at their 1st session on 20-21 January 1997 at the IOC/UNESCO headquarters in Paris, it was decided to start MedGLOSS by launching a pilot network monitoring system. The Joint Group of Experts noted that the IOC

Black Sea Regional Committee at its First Session (September 1996) had recommended to initiate a Black Sea sea-level monitoring programme in association with GLOSS, with emphasis on coastal regions subject to flooding and sea-level rise impact.

The pilot network was initially planned to include some 27 stations in 13 countries which have expressed their interest in joining this international research network. Inclusion of additional stations/countries to the pilot phase by other countries could be considered if they answered the requirements of the pilot stations. Details were provided in the summary document on MedGLOSS prepared by the author in February 1997. The pilot network was intended to become operational and provide initial useful results during 1998, to serve as a model to all countries along the coasts of the Mediterranean and Black Seas, with respect to the attributes and gainsxpected by all Mediterranean and Black Seas countries joining the MedGLOSS. The pilot network consists of the five GLOSS sea-level monitoring stations available in the basin area, and a limited number of sea-level monitoring stations located in countries which expressed their interest in joining MedGLOSS. The pilot plan called for a minimum of two visits of 3-5 days GPS missions and absolute gravimetry at all selected sites, of which a limited number were planned to become permanent GPS stations. The sea-level stations should provide hourly sea-level and atmospheric pressure data daily, via near real-time monitoring, communication and presentation system. The preliminary outcome of the data processing and applications were planned to be presented at the CIESM Congress in Dubrovnik which took place June 1998, with the intention to invite at that time all Mediterranean and Black Seas bordering countries to join the MedGLOSS network.

2. Progress of Pilot Network Set-up

During 1997 contacts were established with the 13 countries listed in Table 1 attached here. Later on requests from two more countries (Romania and Georgia) for joining the MedGLOSS pilot network were received. In June 1997 a joint IOC-CIESM training workshop on sea-level observations and analysis for the countries of the Mediterranean and Black Seas was held at the Proudman Oceanographic Observatory in UK. It included trainees from Algeria, Bulgaria, Croatia, Egypt, Morocco, Romania, Turkey and Ukraine which enjoied the lectures of a number of invited experts and of POL experts. The writer presented the trainees the MedGLOSS programme and established direct contacts with the participants. An additional course in accurate benchmark leveling for sea-level reference and plate tectonics movements detection was held under the leadership of Prof. Suzanna Zerbini in Kos, Greece.

Following these workshops, the writer presented an update of the needs of the various countries which expressed interest in joining MedGLOSS. All resumed to some way or another in requesting some financial support. On the basis of the status of the various stations selected for

the pilot stage, it was estimated that a sum of about $300,000 will be needed to cover the cost of upgrading some of the sea-level monitoring stations and especially for the combined GPS/accurate gravimetry missions. It became clear that the IOC and CIESM can not provide so large funds, so an effort was done by Suzanna Zerbini and Dov Rosen to prepare proposals for funding from European research programs in fall 1997 and winter 1998. These however unsuccessful as the time schedule for the submission of the proposals could not be met due to lack of partners from Egypt or Tunisia in one proposal with Italy and Israel, or too late arrival of another final proposal for submission (with United Kingdom, Israel, Ukraine and Georgia). At the CIESM Congress held in Croatia in June 1998, the importance of MedGLOSS was again reaffirmed, and CIESM commitment to MedGLOSS was reconfirmed. CIESM decided to support the upgrading of 4 sea-level stations in 4 member countries, namely Romania, Croatia, Egypt and Tunisia which were considered of higher priority in provision of sea-level data at regions lacking any digital stations for near-real time data transfer. Matching for the measurement of the benchmarks by accurate GPS and gravimetry were expected to be provided by IOC, but so far these were not received. However, with the recent occupation of the IOC position held in the past by Dr. Albert Tolkatchev by Dr. Thorkild Aarup, Programme Specialist it is expected that IOC once again will join forces with CIESM in the advancement of MedGLOSS, including provision of funds. The countries adhering to the MedGLOSS pilot network, have been requested to commit themselves for long-term maintenance of the sea-level stations, for submission of the near-real time sea-level and atmospheric pressure data to the temporary MedGLOSS centers established at Israel Oceanographic and Limnological Research, National Institute of Oceanography (sea-level verification and redistribution), the satellite sea-level monitoring station of the Collecte-Localisation-Satellite (CLS), Direction Oceanographie Spatiale in Toulouse as well as to the PSMSL in UK and at the University of Bologna for GPS Sea-Level Bench Marks data.

After contacts with the Tunisian authorities, it was decided by them that Tunisia will set-up on its own funds a sea-level station according to the MedGLOSS standards. At present time it is yet not clear when its integration in the MedGLOSS pilot network will be effected. Consequently, CIESM decided to install the equipment of the available sea-level station to Malta. Official commitments to join MedGLOSS pilot network (including data transmission and long-term maintenance and operation) have been received from Romania, Croatia and Malta, while from Egypt are yet to be received, although positive expression to join was given. Consequently, at present purchase and installation of digital sea-level stations equipped as recommended by the MedGLOSS Joint Group of Experts (digital sea-level and atmospheric pressure sensors, data gathering computer with modem) are underway for Romania, Croatia and

Malta, and they are expected to become fully operational before the end of the milenium. At the recent EuroGOOS Conference and MedGOOS MOU signing in Rome in March 1999 Dov Rosen presented the participants the MedGLOSS pilot programme, and there were preliminary plans for submitting a proposal jointly by a number of states to the V Framework Programme of the European Union for supporting MedGLOSS programme. CIESM covered the participation of Dov Rosen to the EuroGOOS and MedGOOS meeting in Rome. It has also covered the participation of Dov Rosen, of a sea-level scientist from Romania and jointly with IOC of a sea-level scientist from Ukraine to the Conferences on Sea-Level and to the GLOSS Group of Experts Meeting held both in Toulouse in May 1999. Furthermore, it was recently agreed between CIESM and IOC to fund a new MedGLOSS Conference in spring 2000, to be hosted by the Israel Oceanographic & Limnological Research in Haifa. The Conference will bring together scientists representing the countries which expressed their committment to join MedGLOSS pilot network programme, in order to reach decisions in regards to the near-real time operation of the network.Prior to the Conference, it is intended to hold a 1 day update workshop on sea-level measurement and analysis methods and geodetic fixing of sea-level bench marks, to be performed with the aid of a number of international experts. Details on the Conference are expected to be published by the end of October 1999, so it is expected that they will be made available to the MEDGOOS participants during the MEDGOOS meeting in Rabat. The major outcome of the Conference are expected to be the start-up of full operation of the near-real time MedGLOSS pilot network and attraction to other countries to join MedGLOSS, realizing their immense benefits by doing so.

2. Conclusions

integration of MedGLOSS near-real time sea-level ground true data with the Mediterranean Forecasting System (MFS) has been recognized at the Malta workshop in December 1997. It will be used for providing the ellipsoid to geoid corrections in the sea-level real time satellite elevations measurements, without which the flow gradients fed to the oceanographic numerical models run in these basins may be wrongly determined. It is hoped that the end of the millenium will become a time pivot point in the progress of MedGLOSS. The recent confirmation of the increased rate of melting of the ice cover over Greenland published in Nature this February and the hot 90's period with the climax in 1998 (so far, perhaps jointly by El-Nino and global warming) show that MedGLOSS is becoming a very important means of knowledge and tool for decision making in regards to long term planning in the marine environment and at the coasts of the Mediterranean and Black Seas (particularly in the southern part of the Mediterranean and certain parts of the Black Sea, which seem that could be potentially more affected by sea-level

rise). Hence, continued support by CIESM and IOC and the countries joining MedGLOSS should be given high priority and adequate support.

MedGLOSS site has the map of the network of the sea level measurements in the Mediterranean and Black seas and examples of records.

3.1.1.2. Models and data assimilation

A model of marine dynamics or ecosystem is considered as an important tool of operational oceanography. Dynamical models are based now mainly on the primitive equations which are presented on Fig. 1.

Governing Equations

$$\frac{\partial u}{\partial t}-(\xi+f)v+w\frac{\partial u}{\partial z}=-\frac{1}{\rho_0}\frac{\partial(P+E)}{\partial x}-\nu_H\Delta^2 u+\frac{\partial}{\partial z}(\nu_v\frac{\partial u}{\partial z}), \quad (1)$$

$$\frac{\partial v}{\partial t}+(\xi+f)u+w\frac{\partial v}{\partial z}=-\frac{1}{\rho_0}\frac{\partial(P+E)}{\partial y}-\nu_H\Delta^2 v+\frac{\partial}{\partial z}(\nu_v\frac{\partial v}{\partial z}), \quad (2)$$

$$\frac{\partial u}{\partial x}+\frac{\partial v}{\partial y}+\frac{\partial w}{\partial z}=0, \quad (3)$$

$$\partial P/\partial z=g\cdot\rho, \quad \text{(a)} \qquad P=g\cdot\rho_0\varsigma+g\int_0^z\rho dz, \quad \text{(b)} \quad (4)$$

$$\frac{\partial T}{\partial t}+\frac{\partial(uT)}{\partial x}+\frac{\partial(vT)}{\partial y}+\frac{\partial(wT)}{\partial z}=K_H\nabla^2 T+\frac{\partial}{\partial z}(K_v\frac{\partial T}{\partial z}), \quad (5)$$

$$\frac{\partial S}{\partial t}+\frac{\partial(uS)}{\partial x}+\frac{\partial(vS)}{\partial y}+\frac{\partial(wS)}{\partial z}=K_H\nabla^2 S+\frac{\partial}{\partial z}(K_v\frac{\partial S}{\partial z}), \quad (6)$$

$$\rho=\varphi(T,S). \quad (7)$$

Fig. 1. Primitive equations of the general ocean circulation model.

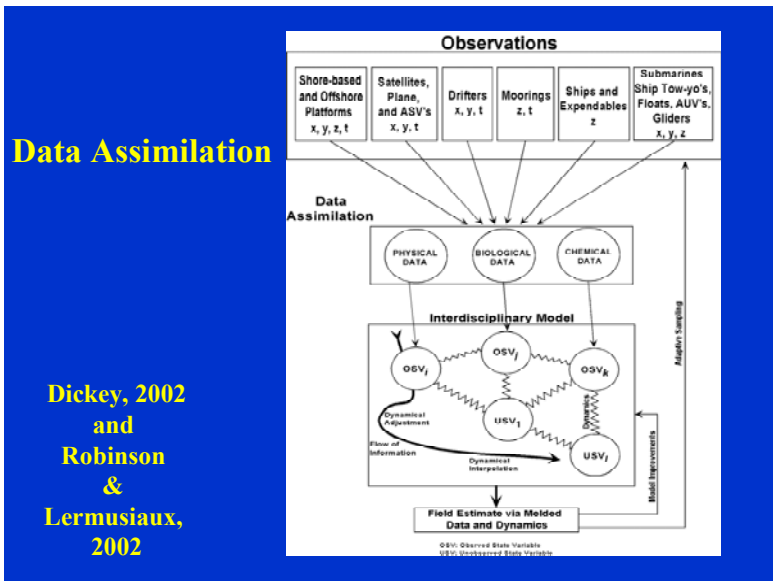

Fig. 2. Data assimilation by the interdisciplinary model.

Differential equations in partial derivatives are presented by finite-differences and are solved by computer. Models of operational oceanography are able to assimilate all operational observations described above according to the scheme presented on Fig. 2. Different kind of data assimilation technique could be used: nudging, optimal interpolation, Calman filter, variational data assimilation.

Models with data assimilation facilities is able to integrate the heterogeneous observations and interpolate them by the optimal way to provide interdiciplinarty nowcasting. Also models are able to predict marine environment changes.

Some models of marine dynamics like POM, HYCOM are available through internet (see web sites below).

http://www.aos.princeton.edu/WWWPUBLIC/htdocs.pom/

http://oceanmodeling.rsmas.miami.edu/hycom/

Some information about HYCOM is presented below.

Evaluation of vertical coordinate and vertical mixing algorithms in the HYbrid-Coordinate Ocean Model (HYCOM)

George R. Halliwell

MPO/RSMAS, University of Miami, 4600 Rickenbacker Causeway, Miami, FL 33149, USA

Abstract

Vertical coordinate and vertical mixing algorithms included in the HYbrid Coordinate Ocean Model (HYCOM) are evaluated in low-resolution climatological simulations of the Atlantic Ocean. The hybrid vertical coordinates are isopycnic in the deep ocean interior, but smoothly transition to level (pressure) coordinates near the ocean surface, to sigma coordinates in shallow water regions, and back again to level coordinates in very shallow water. By comparing simulations to climatology, the best model performance is realized using hybrid coordinates in conjunction with one of the three available differential vertical mixing models: the nonlocal K-Profile Parameterization, the NASA GISS level 2 turbulence closure, and the Mellor–Yamada level 2.5 turbulence closure. Good performance is also achieved using the quasi-slab Price–Weller–Pinkel dynamical instability model. Differences among these simulations are too small relative to other errors and biases to identify the "best" vertical mixing model for low-resolution climate simulations. Model performance deteriorates slightly when the Kraus–Turner slab mixed layer model is used with hybrid coordinates. This deterioration is smallest when solar radiation

penetrates beneath the mixed layer and when shear instability mixing is included. A simulation performed using isopycnic coordinates to emulate the Miami Isopycnic Coordinate Ocean Model (MICOM), which uses Kraus–Turner mixing without penetrating shortwave radiation and shear instability mixing, demonstrates that the advantages of switching from isopycnic to hybrid coordinates and including more sophisticated turbulence closures outweigh the negative numerical effects of maintaining hybrid vertical coordinates.

Interdisciplinary models are coupled together to form a complex system. The scheme of the Harvard Ocean Prediction system is presented on Fig. 3.

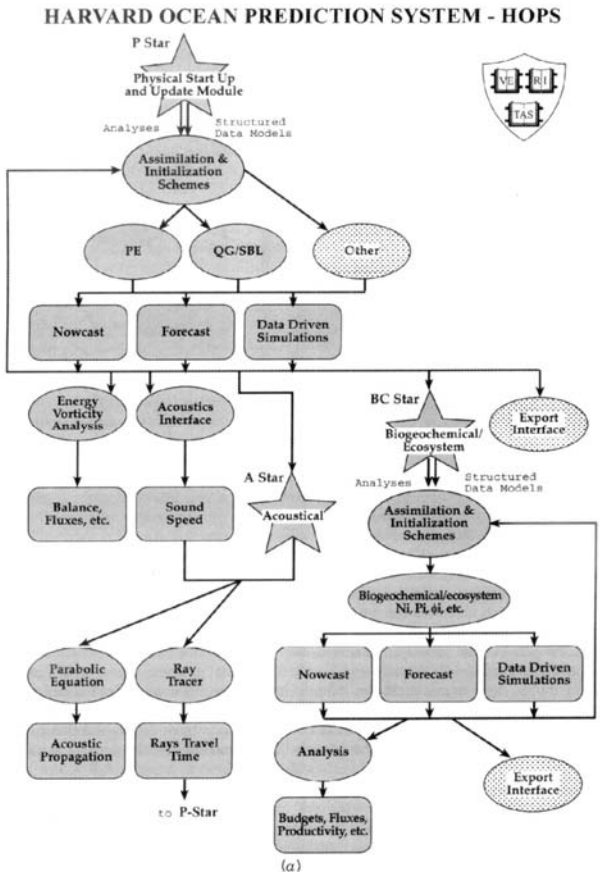

Fig. 3. The scheme of the Harvard Ocean Prediction System.

3.1.1.3. GODAE

The Global Ocean Data Assimilation Experiment (GODAE) is an attempt to apply the concept of operational oceanography to the World Ocean. Some information about GODAE is presented below.

1. Introduction

In early 1997, the Global Ocean Data Assimilation Experiment (GODAE) concept emerged from discussions of the Ocean Observation Panel for Climate (OOPC) with the Committee on Earth Observing Satellites (CEOS) and its Integrated Global Observing Strategy.

The concept was developed in the belief that attracting the resources necessary for an adequate long-term global ocean observing system for monitoring the ocean depends upon a clear demonstration of the feasibility and value of such a system (Smith and Lefebvre, 1997). Using the First GARP Global Experiment (FGGE) as a model, OOPC proposed GODAE as an experiment in which a comprehensive, integrated observing system would be established and held in place for several years and the data assimilated into state-of-the art models of the global ocean circulation in near real-time.

2. The vision

Progress across a wide range of ocean research and applications depends upon the prompt and dependable availability of ocean information products. Recent scientific and technical progress suggests that significant improvement in the quality of these marine services is feasible. However, a coordinated international effort is required to achieve this improvement. The Global Ocean Data Assimilation Experiment (GODAE) seeks to provide a framework for this effort. The vision is

"A global system of observations, communications, modeling and assimilation, that will deliver regular, comprehensive information on the state of the oceans, in a way that will promote and engender wide utility and availability of this resource for maximum benefit to the community."

GODAE aims to make this concept a reality, making ocean monitoring and prediction a routine activity in a manner similar to weather forecasting. GODAE will contribute to an information system for the global ocean that will serve interests from climate and climate change through to ship routing and fisheries.

GODAE will create the conditions for an efficient and effective global ocean measurement network, provided through a variety of direct and remote methods, and sustained for the long-term on the basis of demonstrated, practical utility. The raw and processed information (data and analyses) are distributed globally via a system of communications and data serving that satisfy the demand for immediacy and timeliness of information, in a way that makes clear the character and quality of data sets.

3. Rationale and Objectives

The rationale behind GODAE recognizes both societal need and scientific and technical opportunity. There is an accepted demand for an efficient, integrated system for global ocean products, provided regularly, and in real-time. Recent scientific and technical progress suggests the solutions to this demand are now both feasible and affordable. The underlying rationale for GODAE as an international experiment is that the vision will not be realized serendipitously. The needed capacity will not be realized without a concerted effort to ensure, first, proper integration of the components and, second, the commitment to proving value and viability.

The specific objectives are to:

I Apply state-of-the art ocean models and assimilation methods to produce short-range open-ocean forecasts, boundary conditions to extend predictability of coastal and regional subsystems, and initial conditions for climate forecast models.

II Provide global ocean analyses for developing improved understanding of the oceans, improved assessments of the predictability of ocean variability, and as a basis for improving the design and effectiveness of a global ocean observing system.

The specific goals are to:

1. Coordinate and foster a more efficient, responsive and sustainable system for data assembly, quality control and access.
2. Improve public access to and awareness of the many marine services products, both operational and research that are available.
3. Foster the development of a shared "Common" of ocean information and tools for the production of improved ocean products.
4. Foster the production and analysis of improved ocean service products.
5. Undertake experiments to assess the utility of various ocean data streams for different applications.
6. Guide the evolution of a global ocean observing system, until the system and tools are able to produce ocean service products that meet the needs of the GODAE sponsors.

GODAE will address such questions as

- What accuracy, skill and value to users is achievable with present state-of-the-art observation, modeling and assimilation techniques for analyses and forecasts of (a) the mixed-layer (out to 3-5 days ahead), (b) the ocean mesoscale (out to 10-20 days ahead), and (c) seasonal and longer-term variability?
- What use can be made of these open ocean analyses and forecasts to improve the accuracy and value of (a) estimates of currents and their variability along the shelf break, and (b) analyses and forecasts of waters on the continental shelf?

The objectives are intentionally broad in the belief that wide utilization and exploitation are essential ingredients for cost-efficiency and relevance to society. There is also the desirable balance between the practical and applied goals and the long-term strategic objectives. The scope is determined by the complementary and synergistic areas of real-time, high-resolution, operational oceanography and near real-time climate applications. The essential fields are ocean temperature, velocity, sea level and salinity.

More information could be found on the site
http://www.bom.gov.au/bmrc/ocean/GODAE/